Construction and Building Materials 409 (2023) 134009

Contents lists available at ScienceDirect

Construction and Building Materials

journal homepage: www.elsevier.com/locate/conbuildmat

Structural response of steel sandwich panels with PUR foam core subjected to edgewise compression: Experimental, numerical, and analytical considerations

Pier Giovanni Benzo, João M. Pereira, José Sena-Cruz *

University of Minho, ISISE, ARISE, Department of Civil Engineering, Guimarães, Portugal

ARTICLE INFO

Keywords:
Sandwich panel
Cold-formed steel
Digital image correlation
Edgewise compressive test
Wrinkling
Geometrical imperfections

ABSTRACT

With the objective of leading to innovative lightweight structural components in the construction sector using sandwich panels with polyurethane foam and steel face sheets, different studies were conducted on such structures, including experimental, numerical, and analytical campaigns. The experimental campaign includes the mechanical characterisation of the constituent materials and the edgewise compressive test of small-scale sandwich panels. The test protocols are detailed, and their influence on the results is assessed. Through the use of digital image correlation recordings, deformation patterns and failure mechanisms in the constituent materials and the composite structure are identified. Material constitutive models are calibrated based on the experimentally obtained results. The accuracy of such models is first evaluated against the stress–strain curves recorded during the experiments. In the second stage, the response of the sandwich panels subjected to edgewise compressive loading is simulated. A parametric analysis on the sensitivity of the numerical models to the initial geometrical imperfections is shown to be fundamental to capturing the behaviour of the sandwich panels. Furthermore, the experimental and numerical results are compared to analytical solutions of the problem of the edgewise compression of sandwich panels. Finally, a thorough discussion of the obtained experimental, numerical and analytical results is presented, along with comparisons to results available in the literature.

1. Introduction

The use of sandwich panels as primary structural elements in weight-sensitive applications is expanding through different industries, ranging from aerospace to construction [1]. The widespread use of such structural members is due to the high strength-to-weight ratio deriving from the combination of two thin and stiff face sheets with a relatively thick and less dense core material [2]. A large number of different combinations are possible, and thus, a wide range of properties can be achieved to best address the design requirements of the sought application [3]. In civil engineering, sandwich panels also offer the possibility of combining structural and building physics features. The face sheets and web materials provide the required structural performance, whereas the core material generally provides the necessary thermal and acoustic insulations [4]. Furthermore, the core is responsible for transferring stresses from one face sheet to the other, ensuring the monolithic behaviour of the sandwich panel. The reduced weight allows for ease of transportation and installation as well as faster construction time [5]. Such qualities are highly sought-after in new trending civil engineering sectors, such as the rehabilitation of existing buildings. The practice of reuse of existing buildings contributes positively to the reduction of construction waste, preservation of cultural heritage, and reduction of urban sprawl and the use of non-sealed soil [6].

Composite and metal face sheets sandwich panels show potential to be used as lightweight floor systems for the rehabilitation of existing buildings. The former category involves mostly the use of glass fibre-reinforced polymer (GFRP) face sheets and polymeric foam cores. However, the virtuous use of recycled materials is also found in the literature [7] as well as attempts to include natural fibres in GFRP laminates [8]. The studies of the flexural behaviour of composite sandwich panels [4,5,9–11] highlighted some critical aspects, including high shear deformability of the core materials, brittle failure modes with complete loss of resistance at failure initiation, and face sheet-to-core debonding due to debris resulting from machining of polymeric foam blocks. The latter category includes the use of cold-formed steel (CFS) and mostly low-density polyurethane (PUR) foam. The production

* Corresponding author.
E-mail address: jose.sena-cruz@civil.uminho.pt (J. Sena-Cruz).

https://doi.org/10.1016/j.conbuildmat.2023.134009
Received 7 July 2023; Received in revised form 2 October 2023; Accepted 28 October 2023
Available online 17 November 2023

technology involves the injection of liquid prepolymer into the CFS face sheet or mould. As polymerization and cross-linking occur an adhesive bonding is achieved between the face sheets and the core [12]. The research on steel web-core sandwich panels infilled with PUR foam have focused on their application in roofing system [13,14] showing that instability phenomena govern the ultimate failure of such structures. Furthermore, another critical aspect in the literature is the characterisation of the PUR foam core of CFS panels and profiles. The heterogeneity deriving from the manufacturing process makes the contribution of the PUR foam core to the mechanical resistance difficult to estimate [15,16].

In the context of the development of sandwich panels for civil engineering applications, the edgewise compressive test is often considered the first step to evaluating the load-carrying capacity of the composite structure [1,9,17].

The use of woven E-glass fibre face sheets sandwich panels with different core designs as primary structural elements is studied in [18]. The study highlights the beneficial effect of reinforcement in the core in terms of axial strength. Several failure modes for the edgewise compressive tests are identified. The results of the developed numerical models are in good agreement with the experimental data of the three-point bending test.

The axial response of glass fibre reinforced polymer (GFRP) face sheet sandwich panels with polyisocyanurate (PIR) foam core to be used as prefabricated wall, roof, and deck systems is studied in [1]. A set of specimens with different core densities and slenderness ratios are tested in edgewise compression configuration to study those parameters' influence on the sandwich panel's response. The average peak loads are compared to the analytical predictions of global buckling load accounting for the presence of a soft core with an overall good agreement.

The debonding failure between core and face sheets of sandwich panels for rapid assembly building is addressed in [7]. High-density polyethylene face sheets with studs on the inner surface are used to increase the strength of the face sheet-to-core interface. A comparison between the experimental and numerical results of the edgewise and flatwise compressive tests is presented. However, little information is provided regarding the constitutive models of the materials.

A comprehensive study on the constituent material, as well as the axial and flexural behaviours of sandwich panels for building floors and footbridge decks, is presented in [9]. The sandwich panels have GFRP face sheets, while different materials and core configurations are studied. Edgewise compressive tests are performed, and axial compressive stiffness and strength are determined.

In aerospace, naval, and automotive sectors, edgewise compressive tests are also carried out to assess the response of lightweight sandwich panels. A thorough analytical study, including the construction of collapse mechanisms maps, is carried out in [19] and [20]. The analytical predictions are validated against the results of experimental tests on sandwich panels with varying aspect ratios. According to [19], analytical formulas are more accurate for sandwich panels with higher core density and specimen length. Analytical estimations are also compared to the results of edgewise compressive tests on sandwich panels with GFRP face sheets and different polymeric foams in [21]. The formulas generally overestimate the axial strength, and it is suggested that this may be due to initial geometrical imperfections in the specimen. The buckling behaviour of a honeycomb foam-filled sandwich panel with GFRP face sheets, is investigated in [22]. Numerical models considering the viscoelastic and elastic properties of the constituent materials. The viscoelastic models show smaller differences with the experimental load-displacement curves.

FRP face sheets sandwich panels are extensively studied in the literature. However, there is a lack of knowledge on the behaviour of steel face sheets sandwich panels for primary structural applications in civil engineering. Furthermore, fewer numerical and analytical studies of sandwich panels for civil engineering applications are found compared to those in aerospace, naval, and transport sandwich constructions. This paper addresses the above-mentioned gaps in the literature.

In the scope of the LightSlab R&D Project, a new floor system based on sandwich panels is proposed. The sandwich panel comprises cold-formed steel face sheets with a polyurethane (PUR) closed-cell foam core reinforced by cold-formed steel webs. Steel insulating sandwich panels are already a mature product in the construction sector, but their applications have been limited to secondary structural elements, i.e. façade and roofing systems. The initial cost of FRP materials in civil engineering is generally higher than steel [23–25], therefore steel face sheets sandwich panels represent an economic competitive solution. As mentioned before, steel-insulated sandwich panels can be already produced continuously and with a high level of quality control. Further information on the preliminary design and the optimisation process by means of genetic algorithms (GA) of the novel sandwich panel cross-section is available at [26]. In this paper, the first stage of the experimental campaign envisaged for the development of the new lightweight floor system is presented. The experimental programme includes the mechanical characterisation of the constituent materials and the edgewise compressive tests on small-scale sandwich panels without longitudinal webs. The tests on the small-scale sandwich panels are carried out to preliminarily assess the composite element's structural integrity. The experimental results are then compared to analytical and numerical models to provide insight on the mechanical response of the sandwich panel.

2. Experimental campaign and specimen manufacturing

Through an optimisation procedure based on GA, the optimal physical and mechanical properties of the constituent materials, as well as the optimal cross-section geometry, were determined [26]. The optimised cross-section of the full-scale prototype is shown in Fig. 1(a). The face sheet and webs are made of continuous hot-dip zinc-coated carbon steel sheets with a yielding and ultimate strength of 220 MPa and 300 MPa, respectively. The core is made of PUR foam with a density of 40 kg/m^3 to provide the necessary thermal insulation required by the Portuguese building code [27]. Technical delivery conditions are available for the steel sheet from where the coupon specimens were machined. Uniaxial tensile coupon tests are carried out to verify the mechanical properties of the steel. On the other hand, no information was provided on the mechanical properties of the PUR foam by the sandwich panel manufacturer. Thus, flatwise compressive and tensile tests are performed to mechanically characterise the core material. Finally, edgewise compressive tests are carried out on small-scale sandwich specimens to gain insight into the response of the composite structure.

Specimens for both the flatwise compressive and tensile tests and edgewise compressive tests are manufactured in the same fashion. The samples are cut off from larger sandwich panels whose production is illustrated in Fig. 1(b). The stages of the manufacturing process are the following: i) cold-formed steel sheets are unrolled from the coil and fed into the conveyor belt of the continuous production line; ii) the liquid monomers of the PUR foam are injected on the bottom face sheet of the sandwich panel; iii) the top face sheet is pressed on top of the expanding PUR foam; v) the sandwich panel is heated up to 40 °C to speed up the curing of the PUR foam. The integrity of the composite structural member is ensured by the adhesive bond between the steel face sheets and the PUR foam. The adhesion results from the polymerisation and cross-linkage occurring in the liquid monomers of the PUR foam once they are injected into the face sheets. Indeed, this manufacturing process avoids dust and debris resulting from the cutting of PUR foam blocks, which may hinder the face sheet-to-core interface strength [28].

In the following sections, a detailed description of the protocols, setup, and results of the tests carried out in the Structural Laboratory of Civil Engineering (LEST) facility of the University of Minho will be presented. The following tests were performed: i) coupon tensile tests of

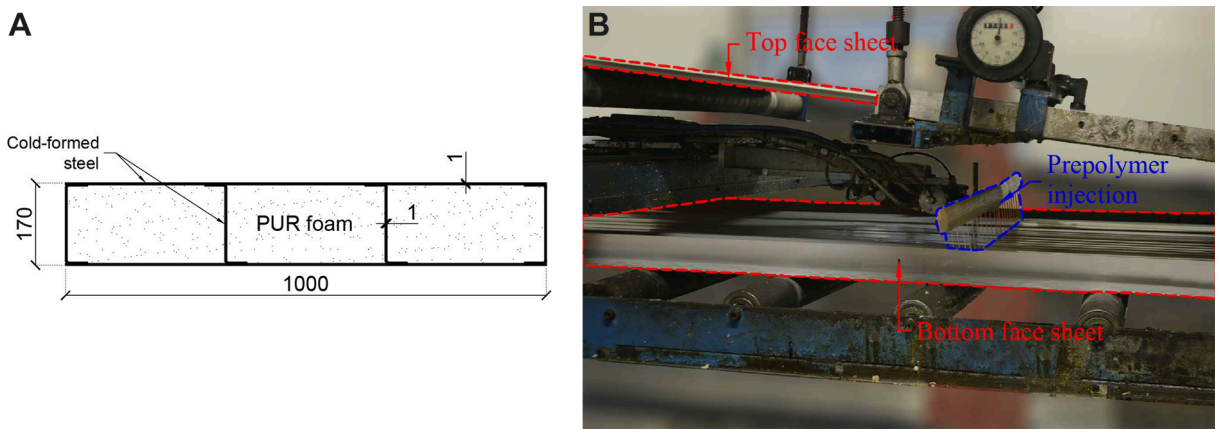

Fig. 1. Development of the sandwich panel: (a) final cross-section obtained through GA optimisation procedure [26]; (b) current manufacturing process. Note: units in [mm].

steel; ii) flatwise compressive and tensile tests of the PUR foam; iii) edgewise compressive tests of small-scale sandwich panels.

2.1. Tensile coupon tests

Tensile coupon tests were carried out according to ISO 6892-1 (2016) [29] on two sets of specimens with a nominal thickness of 1.0 mm (TC-1.0) and 1.5 mm (TC-1.5), respectively. A preliminary design carried out in [30] demonstrated that the sandwich panels met the structural safety requirements for standard spans in residential buildings within this range of steel sheet thicknesses. The coupon specimens were extracted in the longitudinal direction of the steel sheets used in the production of the sandwich panels. The nominal dimensions of the coupon specimens are identical for sets TC-1.0 and TC-1.5, and are shown in Fig. 2(a).

Prior to testing, gauge marks were applied in the region of interest, and the cross-section dimensions of the specimens were measured with a digital calliper. The coupon tensile tests were carried out in a universal testing machine (UTM) with a capacity of 200 kN. The tensile load is applied by gripping the ends of the specimens with clamps. The overall test setup is shown in Fig. 2(b).

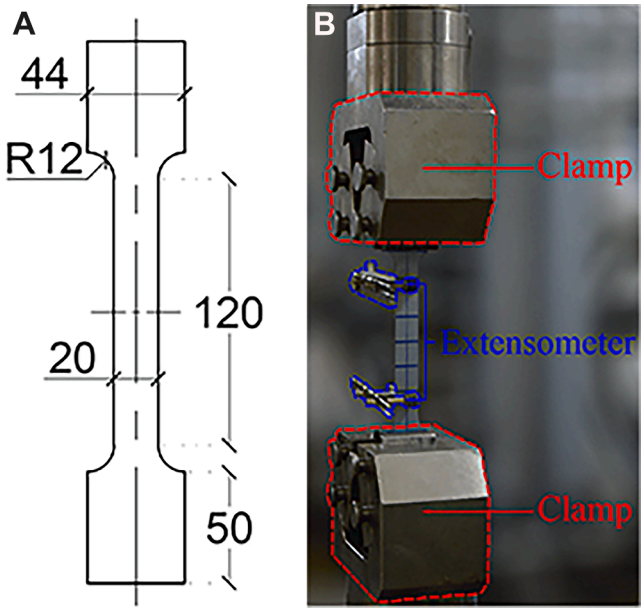

Fig. 2. Steel coupon tensile test: (a) nominal dimensions; (b) test setup. Note: dimensions in [mm].

The coupon specimens were tested in a quasi-static monotonic-instantaneous loading up to failure under displacement control. The displacement-based loading protocol followed the suggestions of [31] to eliminate the influence of the strain rate on the test results. A displacement rate of 0.003 mm/min was applied until reaching the proportional limit. The test speed was then increased up to 0.015 mm/min and kept constant until the yielding phenomenon was completely developed. Finally, the displacement rate is increased to 0.066 mm/min until failure to keep the test duration within a reasonable time. The loading was paused for 100 s at different critical locations to obtain the static drops due to stress relaxation. The pauses were near the 0.2% proof stress, at the beginning of the hardening region, and near the ultimate strength.

2.1.1. Results

The static engineering stress-strain curves for the two sets of specimens are shown in Fig. 3(a). The static curves shown are obtained from the dynamic curves recorded during the experiments according to the method described in [31]. Both sets of specimens present pronounced yielding phenomena according to the definition provided by EN 10346 (2015) [32]. A failed specimen exhibiting the typical necking phenomenon before fracture is shown in Fig. 3(b).

The mechanical properties obtained from the tests are reported in Table 1, including the Young's modulus (E), the yielding strength (σ_y), the ultimate tensile strength (σ_u), and the strain at fracture (ε_f). The two sets of specimens presented similar levels of ductility. The coefficients of variation are generally in agreement with the experimental procedure proposed in [31] (within 8%). The larger scatter found in the elastic modulus may be due to the presence of out-of-straightness defects in the specimen resulting in the introduction of bending moments and a non-uniform state of tensile stresses. The specimens with a nominal thickness of 1.0 mm satisfy the requirements of the steel grade S250GD+Z. On the other hand, the specimens with a nominal thickness of 1.5 mm do not meet the minimum requirements of the steel grade S220GD+Z in terms of yielding strength. Nevertheless, the values reported in Table 1 correspond to the static yielding strength. The mechanical properties reported in the technical data sheets usually refer to the dynamic values established according to the strain rates imposed by the standard [33]. A statistical analysis of the TC-1.0 and TC-1.5 sets of data using the interquartile range (IQR) method was carried out to detect outliers [34]. The elastic modulus of specimen TC-1.5-1 was below the lower inner fence and, thus, identified as an outlier. The low Young's modulus of TC-1.5-1 may be attributable to the out-of-straightness defect observed in the specimen. Additionally, slippage marks could be observed on the clamped regions of specimen TC-1.5-1. This may explain the higher noise level registered in the force reading, resulting in lower accuracy in

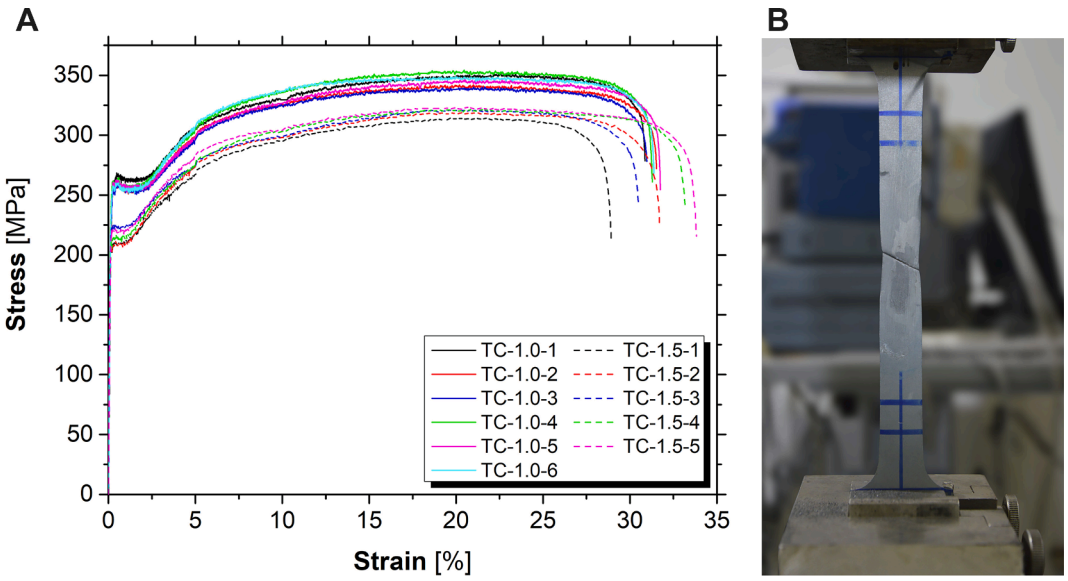

Fig. 3. Uniaxial coupon tensile test result: (a) stress-strain curves; (b) failure mode.

Table 1
Summary of the mechanical properties of the cold-formed steel sheets.

Specimen [-]	σ_y [MPa]	σ_u [MPa]	ε_f [%]	***E*** [GPa]
TC-1.0-1	261	351	30.87	190
TC-1.0-2	253	342	31.54	222
TC-1.0-3	253	340	30.97	201
TC-1.0-4	259	354	31.29	194
TC-1.0-5	258	346	31.75	209
TC-1.0-6	254	349	31.39	214
Avg. (CoV)	256 (1.3%)	347 (1.6%)	31.30 (1.1%)	205 (5.9%)
SD	3	5	0.33	12
TC-1.5-1	210	315	28.93	166*
TC-1.5-2	210	319	31.69	198
TC-1.5-3	225	321	30.51	203
TC-1.5-4	215	321	33.19	190
TC-1.5-5	219	323	33.83	187
Avg. (CoV)	216 (3.0%)	320 (1.0%)	31.63 (6.3%)	194 (3.8%)
SD	6	3	1.99	7

Notes: Avg. – average value per set of specimens; CoV – coefficient of variation; SD – standard deviation; the highlighted outliers with the symbol "*" were not considered in the average calculation.

estimating the elastic modulus.

2.2. Flatwise compressive and tensile tests

Flatwise compressive and tensile specimens were carried out according to ASTM C297 (2004) [35] and ASTM C365 (2003) [36], respectively, on PUR closed cell foam specimens with a nominal density of 40 kg/m^3. The mechanical properties studied are those perpendicular to the face sheets of the sandwich panels, which are particularly relevant in the prediction of local instability phenomena such as wrinkling. The tests were performed on cubic specimens with 60 mm sides. The specimens were cut out from larger sandwich panels with a core thickness of 60 mm and face sheets thickness of 1.0 mm. Before testing, the specimens' dimensions were measured, and their weight was recorded with a scale. Based on that information, the estimated density of the PUR foam is 39.6 kg/m^3, and its relative difference with the nominal density is -1.0%.

The tests were carried out in a UTM under displacement control with a capacity of 25 kN. The vertical displacements were measured by four LVDTs, installed on each face of the cubic specimen to account for possible rotations deriving from the misalignment of the loading plate [37] (see Fig. 4).

The setup pieces accommodating the LVDTs were glued to the face sheets according to the following procedure: i) both the surfaces of the setup pieces and the face sheets of the specimens were polished with sandpaper and cleaned with acetone; ii) a PUR-based two components adhesive was mixed and applied to the setup pieces and the face sheets of the specimens; iii) the coupons and setup pieces were assembled, and the adhesive was cured for 2 h at 40 °C and then for at least 12 h, at room temperature, before the test. Regarding the flatwise compressive test, spherical washers were placed between the specimen assembly and the loading plate to ensure that only axial loading was applied to the PUR foam (see Fig. 4(a)). In the case of the flatwise tensile test, 3D bearing joints were screwed to the setup pieces and connected to the frame and hydraulic actuator to avoid bending moments in the system (see Fig. 4 (b)).

Furthermore, a speckle pattern was applied to one of the specimens' faces for selected specimens to gain insight into the mechanical behaviour of the PUR foam. Digital image correlation (DIC) was employed to monitor the evolution of strains over the selected faces. The flatwise compressive test was carried out at a speed of 2.4 mm/min, whereas the speed of the flatwise tensile test was 0.5 mm/min. Preliminary flatwise compressive tests were carried out, and no significant differences were found between the results of specimens tested at 0.5 mm/min and 2.4 mm/min. Thus, the flatwise compressive tests were carried out at a higher displacement rate to keep the test duration within a reasonable time.

2.2.1. Results

The stress-strain curves of the flatwise compressive and tensile tests are shown in Fig. 5. The compressive stress-strain curves present three distinct regions: i) a linear elastic branch for low levels of strains; ii) a plateau where deformation occurs at a constant level of stress due to the buckling of the cell walls of the PUR foam; iii) a hardening stage involving the densification of the material as a result of the cell walls crushing [38]. For what concerns the tensile stress-strain curves, a linear behaviour is observed up to failure, which occurred by rupture of the PUR foam close to the top face sheet-to-foam interface.

A summary of the mechanical properties obtained from the flatwise compressive and tensile tests on the PUR foam are reported in Table 2, including the Young's modulus in compression (E_c) and tension (E_t), the yielding compressive strength (σ_c) and strain (ε_c), and the ultimate tensile strength (σ_t) and strain (ε_t). E_c and E_t are calculated considering

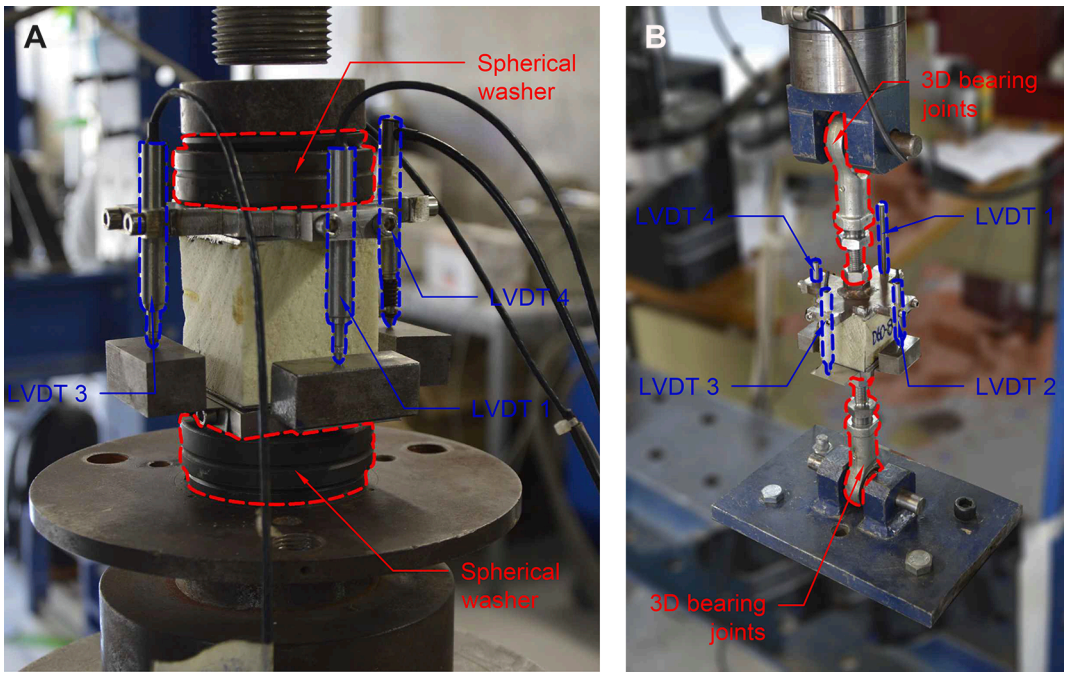

Fig. 4. Mechanical characterisation of the PUR foam: (a) flatwise compressive and (b) tensile test setup.

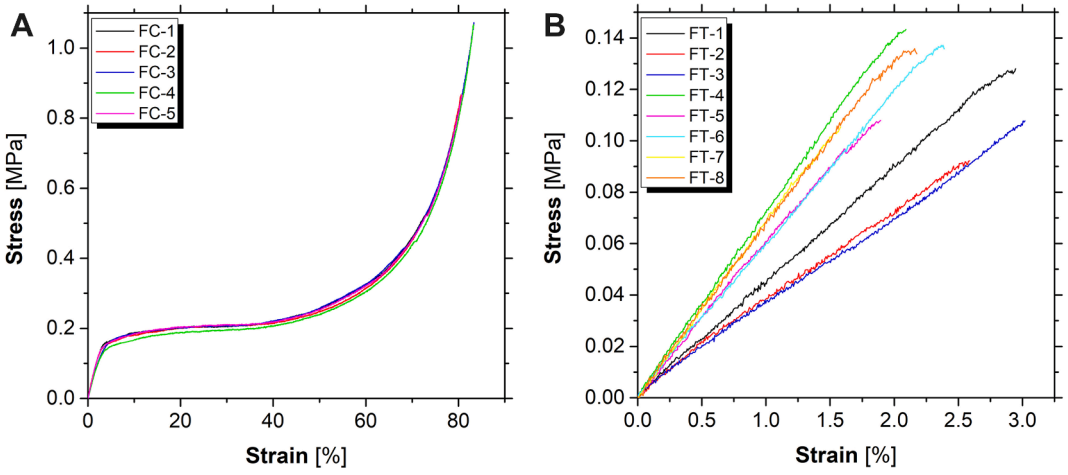

Fig. 5. Stress-strain curves: (a) flatwise compressive test; (b) flatwise tensile test.

Table 2
Summary of the mechanical properties of the PUR foam.

Specimen [-]	E_c [MPa]	σ_c [MPa]	ε_c [%]	**Specimen** [-]	E_t [MPa]	σ_t [MPa]	ε_t [%]
FC-1	6.14	0.153	2.50	FT-1	4.35	0.128	2.95
FC-2	6.23	0.148	2.38	FT-2	4.09	0.092	2.59
FC-3	5.38	0.153	2.84	FT-3	3.65	0.108	3.02
FC-4	5.16	0.138	2.67	FT-4	7.07	0.143	2.09
FC-5	5.99	0.149	2.49	FT-5	6.29	0.108	1.89
				FT-6	5.89	0.137	2.40
				FT-7	6.84	0.105	1.60
				FT-8	6.85	0.136	2.18
Avg. (CoV)	5.78 (8.3%)	0.148 (4.3%)	2.57 (7.0%)	**Avg. (CoV)**	5.63 (24.6%)	0.120 (15.6%)	2.34 (21.2%)
SD	0.48	0.006	0.18		1.39	0.019	0.50

Notes: Avg. – average value per set of specimens; CoV – coefficient of variation; SD – standard deviation.

the slope of the initial part of the elastic stage, i.e. one-third of σ_c and one-third of σ_t, respectively. σ_c is determined as the intersection of the extrapolations of the linear elastic and plateau lines as explained by [39].

The large scatter found in the tensile properties of the PUR foam is within the range of the coefficients of variation reported in other studies [15,40]. The production technology and the mould's size and shape significantly influence the foamed product's microstructure, which in turn determines the macroscopic mechanical properties of the PUR foam [41]. In [16], the location where the specimen is extracted in the full-scale sandwich panel is estimated to contribute 5% of the scatter in the mechanical properties. Furthermore, flaws and defects affect tensile behaviour more than compressive behaviour [42]. Initial defects such as cracks and the presence of large bubbles in the foam may lead to stress concentration in the cell walls, leading to premature failure. The DIC technique can provide further insights into the mechanical behaviour of the PUR foam. The monitored area was divided into three layers, namely the top, middle, and bottom layers (see Fig. 6).

The stress-strain curves corresponding to the different regions across the thickness of the specimens are plotted in Fig. 7, along with the deformation history recorded by the DIC.

Both the flatwise tensile and compressive tests highlight the presence of a more flexible top layer. Such behaviour may be explained by the manufacturing process of the specimen, which determines the foam microstructure. The cell morphology depends on the size and shape of the mould where the liquid monomers of the PUR foam are injected in [40]. The top face sheet constrains the expansion of the foaming mass to obtain the required sandwich panel thickness. This constraint results in an irregular foam microstructure near the top face sheet and, thus, different mechanical properties.

3. Edgewise compressive test

Edgewise compressive tests were carried out according to ASTM C364 (1999) [43] on two sets of specimens with identical nominal dimensions and two nominal thicknesses of the steel face sheet, namely 1.0 mm (EC-1.0) and 1.5 mm (EC-1.5). Specimens with an area of 250 mm x 250 mm were extracted from larger sandwich panels with a core thickness of 100 mm and face sheet thicknesses of 1.0 mm and 1.5 mm. Prior to testing, the specimens were measured and weighted, and an estimated density of 38.8 kg/m^3 was calculated (relative difference from the nominal density of -3.1%). Upon delivery, visible defects were observed in the specimens (see Fig. 8). These defects were a result of the extraction process from the full-scale sandwich panels.

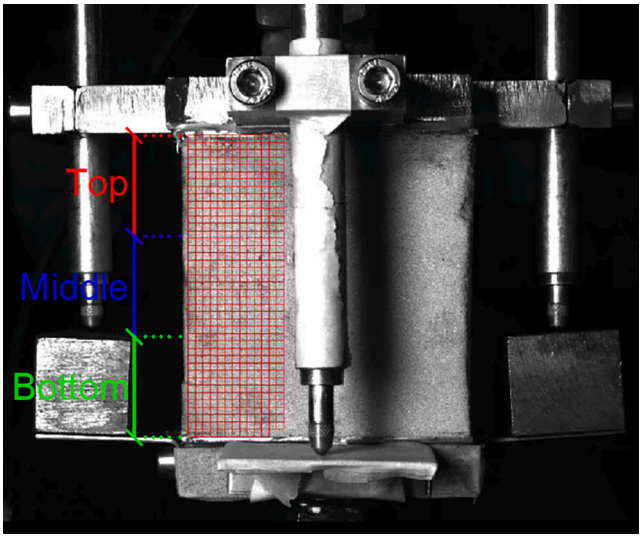

Fig. 6. Area of the PUR foam specimen monitored by the DIC equipment with the corresponding layers.

Various methods were employed to achieve flat end surfaces perpendicular to the length of the specimens. The milling machine produced smooth end surfaces, but induced stress which caused a cohesive crack in the PUR foam parallel to the face sheets (see Fig. 8). Hence, a grinding wheel was deemed more suitable for the smoothing process. The end surfaces' quality was slightly inferior to that achieved with the milling machine, but no cracks in the PUR foam were observed.

The tests were performed in a UTM with a load capacity of 200 kN. The load is transferred through a solid steel 50 mm thick plate to ensure a uniform stress distribution over the loaded region. Prismatic solid steel bars, with a cross-section of 20 mm x 25 mm, were screwed to the plates on the sides of the ends of the specimen to avoid premature failure in the loading and support regions. Vertical displacements were monitored by four LVDTs located on the bottom face of the loading plate to account for possible rotations. Furthermore, one of the lateral faces of the specimen was monitored with DIC. The overall test setup is shown in Fig. 9. The tests were conducted under displacement control at a speed of 0.5 mm/min.

3.1. Results

The results of the edgewise compressive tests for the EC-1.0 and EC-1.5 sets of specimens are shown in Fig. 10.

Generally, both sets present an initial nonlinear part of the curve attributable to the closing of gaps between the loading plates and the ends of the samples. Once the end cross-sections are fully engaged, a linear elastic behaviour is observed until failure initiation.

Different failure modes could be observed in the EC-1.0 specimens as it is noticeable from the high scatter of the results in terms of peak load: i) debonding between core and face sheet (D); ii) global buckling (GB); iii) wrinkling of the face sheets (W). On the other hand, the EC-1.5 specimens present consistent failure mode due to global buckling. In the edgewise compressive test of the EC-1.0 specimen set, there was a significant deviation in the results. This could be due to various factors, such as the extraction process of the specimens from full-scale sandwich panels, resulting in irregular end surfaces and possible cracks in the PUR foam. It is possible that the premature debonding of specimen EC-1.0-1 is due to pre-existing cracks caused by this. Smooth end surfaces could not be achieved due to stress in the bulk of the PUR foam, leading to concentration of stresses and localized end failure. Additionally, the scatter could be attributed to the heterogeneity of the PUR foam and the face sheet-to-core interface, which is crucial for the composite structure's monolithic behaviour [44].

The typical compressive response of an EC-1.0 specimen, along with the deformation history recorded by the DIC, is shown in Fig. 11. The load increases linearly up to 0.3 mm, where a small load drop, corresponding to local instability of the face sheet, can be observed. The load continues to rise until wrinkling of the face sheets occurs. The significant load drop after failure initiation is related to the debonding at the top face sheet-to-core interface. A plateau at constant load is later observed, corresponding to the debonding propagation through the whole surface of the top face sheet-to-core interface. It is possible to estimate the wrinkling half wavelength through the DIC recordings of the specimens that failed due to wrinkling. The average value obtained from specimens EC-1.0-4 and EC-1.0-5 measurements is 65.5 mm (see Fig. 12). DIC recordings of specimen EC-1.0-3 were influenced by lightning conditions, most likely due to changing weather conditions. Because of the above reason, no DIC measurements are available for specimen EC-1.0-3.

The typical progressive deformation and collapse of an EC-1.5 specimen are depicted in Fig. 13. Two distinct linear branches can be observed prior to failure initiation, which is attributed to global buckling. After peak load is attained, a softening branch is observed, corresponding to the formation of a plastic hinge in the top face sheet in the vicinity of the loading plate and the simultaneous crushing of the PUR foam core. The out-of-plane bending of the top face sheet is transmitted

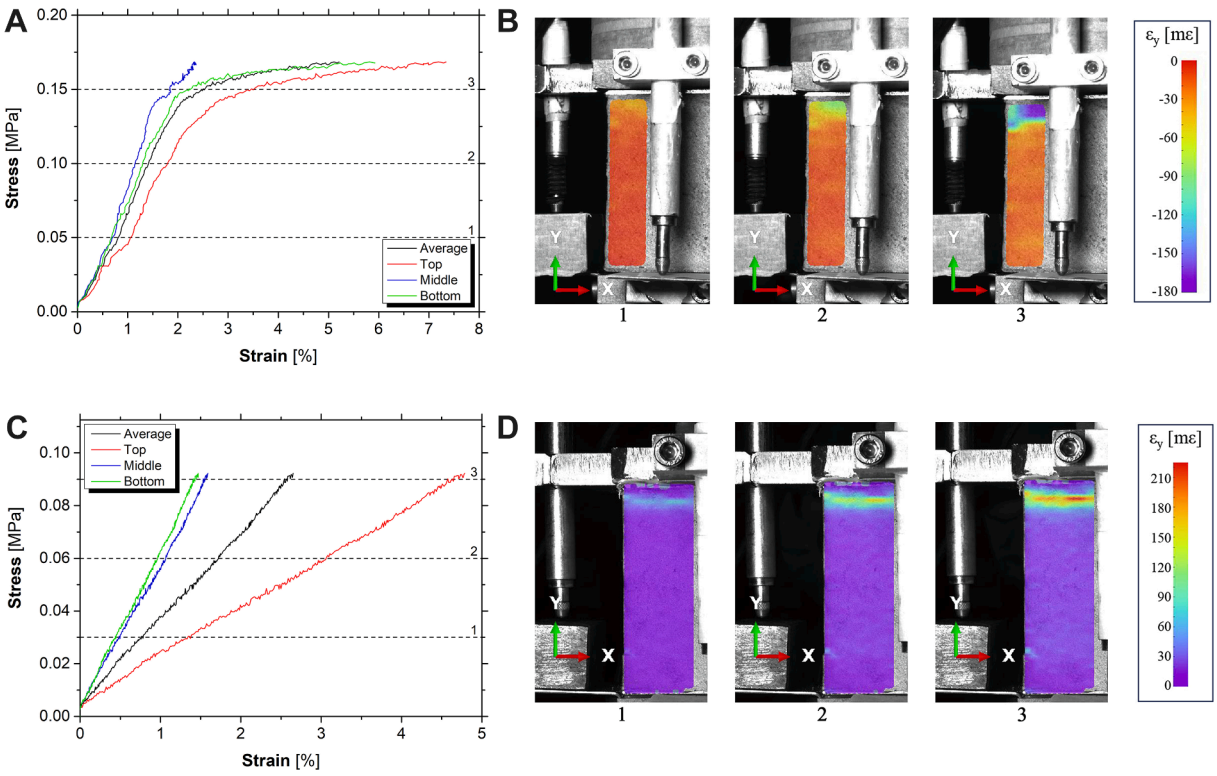

Fig. 7. DIC measurements: (a) flatwise compressive test stress-strain curve and (b) deformation history; (c) flatwise tensile test stress-strain curve and (d) deformation history. Note: units in [millistrain].

to the bottom face sheet through the core. However, the tensile strength of the PUR foam core is not sufficient to hold the face sheets together with the core. A significant load drop is ultimately observed as the bottom face sheet debonds from the core. It is worth noting that most specimens ultimately failed due to debonding of the top face sheet. The inspection of the specimens after testing revealed that a thin layer of PUR foam remained on the debonded face sheet. These results correlate well with the findings of the flatwise tensile test results on cubic sandwich panels specimens. Indeed the tensile tests highlighted the presence of a more flexible layer of PUR foam next to the top face sheet where ultimately the cohesive tensile crack occurred. A summary of the obtained results, including the observed failure modes, are reported in Table 3, namely peak load (P_u), axial stiffness (K), failure initiation, and failure propagation.

The vertical displacement of the cross-sections illustrated in Fig. 14 (a) was tracked by the DIC system. The sampling points of the cross-sections are located in the PUR foam near the face sheet. It is assumed that the deformation of the face sheet and the PUR foam close to the interface is the same until debonding occurs. The DIC's accuracy was validated by comparing the vertical displacement of the cross-section near the loading plate with the LVDTs results. The procedure is illustrated for specimen EC-1.0-4 in Fig. 14(b). The DIC readings could not capture the rotations of the loading plate, which could have caused the small difference (about 10%) from LDVTs measurement, as the DIC only monitors one of the vertical surfaces of the specimen. Moreover, the reading of the loading plate cross-section was influenced and disrupted due to the crushing of the PUR foam, causing damage to the speckle pattern. The plot of the vertical displacement of the top and bottom cross-sections and their relative displacement (Fig. 14(b)) showed that a significant component of the displacement occurred near the loading and supporting areas of the specimens due to the uneven end surfaces of the specimens. The LVDTs measured the relative displacement between the loading and support plates, including the closing of gaps between the specimens and the test setup as well as localised deformations (see Fig. 14(c)). For the reasons mentioned above, the axial stiffness of the sandwich panels was estimated considering the load-displacement curves recorded by the DIC system. However, the axial stiffness values for specimens EC-1.0-3 and EC-1.5-3 could not be estimated because of difficulties encountered during the image-matching process. These challenges were likely caused by varying lighting conditions in the laboratory facility due to changes in weather. This resulted in uneven illumination, which made it difficult for the algorithm to carry out the image correlation process due to insufficient pattern contrast [45].

4. Numerical modelling

Numerical models were developed to replicate the results of the edgewise compressive tests up to failure initiation. For what concerns the EC-1.0 set of specimens, the target of the numerical simulations is to reproduce the most recurrent failure mode initiation, namely wrinkling of the face sheets. On the other hand, numerical simulations of the EC-1.5 specimens were aimed at reproducing the global instability failure mode. Approaches based on the Finite Element Method (FEM) were chosen to perform simulations using ABAQUS 2019 software (ABAQUS). In the first stage, the results of the material characterisation campaign were used to calibrate the constitutive models of the cold-formed steel and PUR foam. In the second stage, finite element (FE) simulations were carried out to match the axial response of the small-scale sandwich panel and provide insight into the strain distribution, the deformation progression, and failure mechanisms. Experimental and numerical results are compared in terms of initial stiffness, peak loads, and deformation pattern.

4.1. Constitutive models

The main goal of this study is the development of numerical models capable of accurately reproducing the mechanical behaviour of the sandwich floor panel. To correctly predict the behaviour of the newly

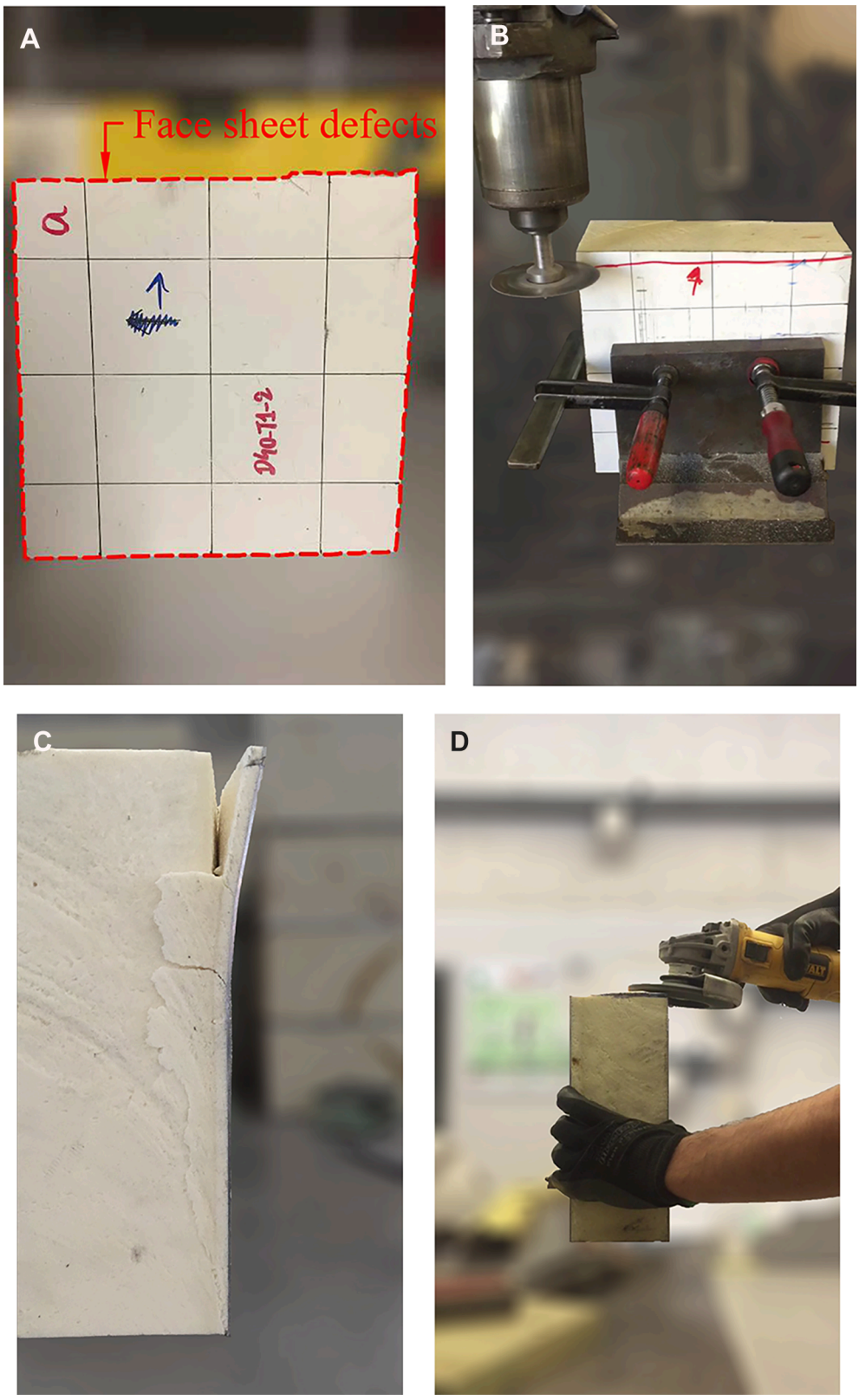

Fig. 8. Sandwich panels specimens upon delivery: (a) face sheet defects; (b) milling machine treatment; (c) cohesive crack due to milling operation; (d) grinding wheel treatment.

developed sandwich panel, the calibration of the face sheet and core materials constitutive models is required. In this section, the calibration methods employed for the cold-formed steel and the PUR foam are described, and the comparison with the material characterisation curves is presented. The nonlinear FE simulations were carried out to match the stress-strain response obtained from the uniaxial tensile test of steel and the flatwise tensile and compressive tests of PUR foam.

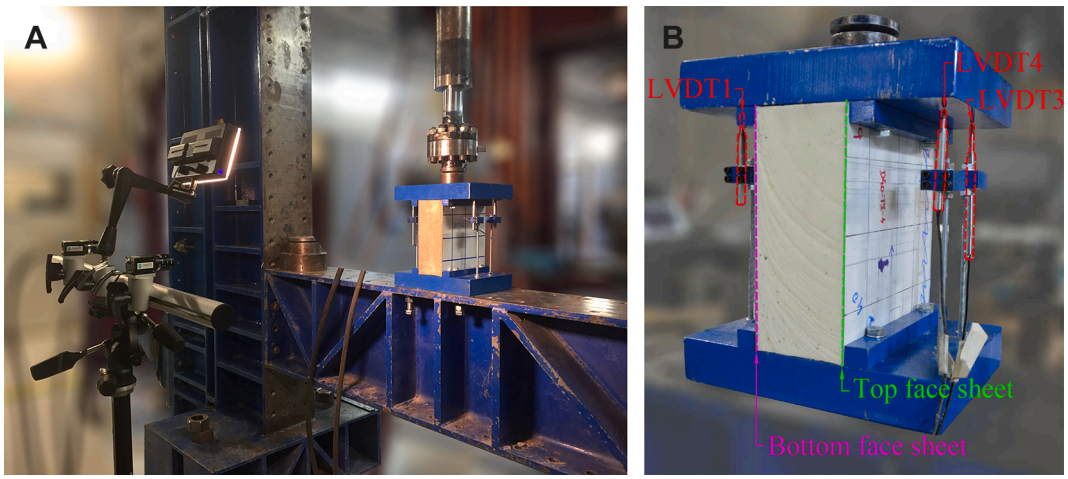

Fig. 9. Edgewise compressive test: (a) overall setup and DIC equipment; (b) specimen.

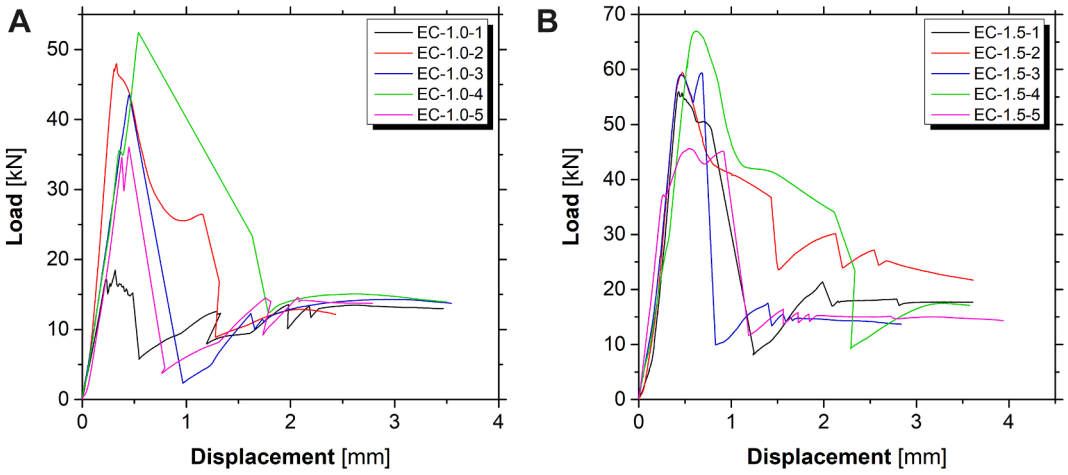

Fig. 10. Edgewise compressive test load-displacement curves: (a) set EC-1.0; (b) set EC-1.5.

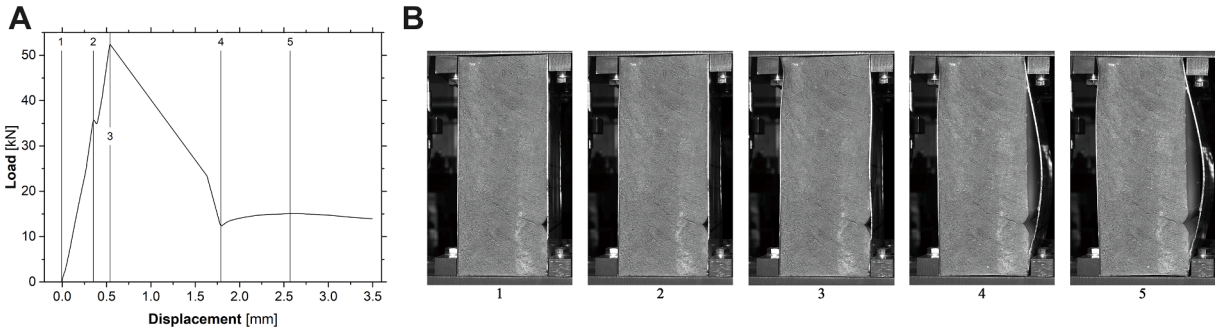

Fig. 11. Edgewise compressive test DIC results: (a) load-displacement curve; (b) deformation history.

4.1.1. Face sheet material

The numerical modelling of steel structures undergoing large deformations requires the estimation of an accurate true stress-strain curve based on a measured engineering stress-strain curve. In this study, the development of the true stress-strain model follows the approach proposed by [46]. An analytical relationship is provided between the engineering stress-strain curve and the true stress-strain curve up to the ultimate tensile strain. The attainment of the ultimate tensile strength is regarded as the initiation of the necking phenomenon in the central region of the coupon. At this stage, highly localised stresses arise in the vicinity of the cross-section undergoing necking. Firstly, a power law is used to fit the stress-strain data in the hardening region. The same power law is then used to extrapolate the true stress from the true ultimate strain up to a true strain equal to 1.0, a typical value for true fracture strain in structural steel, according to [46] and [47]. An advanced FE model with material and geometrical nonlinearity was built to validate the constitutive model to simulate the stress-strain experimental curves. A four-node shell element (S4R) based on linear interpolation and a reduced integration scheme was adopted to model the steel coupon test. The Von Mises yield criterion with isotropic hardening was chosen to

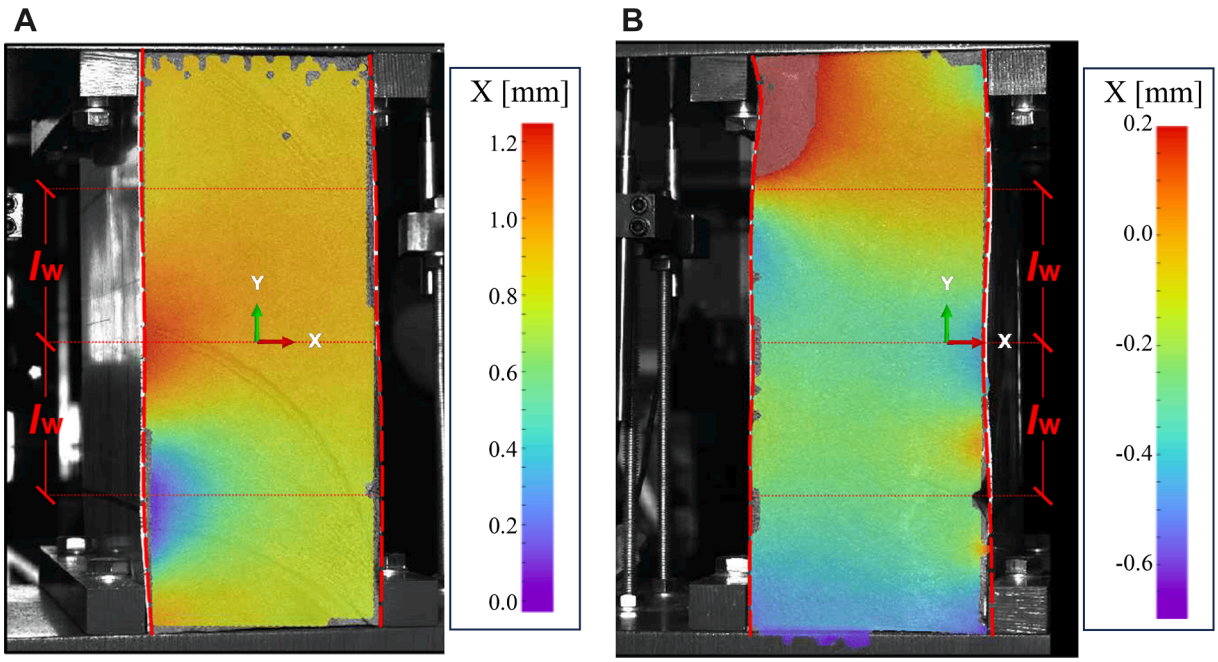

Fig. 12. Wrinkling half wavelength estimation using DIC: (a) EC-1.0-4; (b) EC-1.0-5. Note: units in [mm].

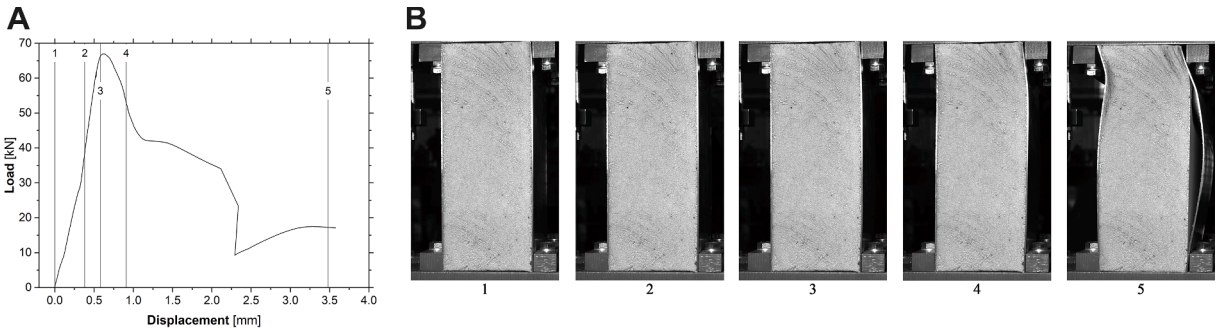

Fig. 13. Edgewise compressive test results: (a) load-displacement curve; (b) deformation history.

Table 3
Summary of the results of the edgewise compressive tests on small-scale sandwich panels.

Specimen [-]	P_u [kN]	K [kN/mm]	**Failure initiation** [-]	**Failure propagation** [-]
EC-1.0-1	18.5	488.3	D (T)	D (T)
EC-1.0-2	48.0	395.1	LB + FC	D (T)
EC-1.0-3	43.5	-	W (T)	D (T)
EC-1.0-4	52.4	520.7	W (T) + FC	D (T)
EC-1.0-5	36.1	592.0	W (T)	D (T)
Avg.	39.7	468.0		
(CoV)	(33.5%)	(17.5%)		
SD	13.3	81.7		
EC-1.5-1	56.0	533.4	GB	D (T)
EC-1.5-2	59.4	503.7	GB	FC
EC-1.5-3	59.4	-	GB	D (T)
EC-1.5-4	67.0	571.2	GB	FC and D (B)
EC-1.5-5	45.6	555.7	GB	FC and D (B)
Avg.	57.5	541.0		
(CoV)	(13.5%)	(5.4%)		
SD	13.5	29.3		

Notes: Avg. – average value per set of specimens; CoV – coefficient of variation; SD – standard deviation; the symbol "-" indicates DIC measurements are unavailable for the specimen.
Failure modes: LB – local buckling; D – debonding; FC – foam crushing; W – wrinkling; (B) – bottom face sheet; (T) top face sheet.

reproduce the metal plasticity. The finite element model's mesh consists of quadrilateral elements, with an approximate side length of 5 mm. In the middle of the model, where the necking phenomenon was observed during experiments (see Fig. 15(a)), there is a more refined area with a side length of 2.5 mm. The end regions' nodes are tied to reference points using the rigid body constraint available in ABAQUS. Therefore, the motion of the clamped parts' nodes in the selected regions is governed by the reference point's motion, and their relative positions remain constant throughout the analysis, i.e. these regions do not undergo any deformation. The bottom reference point was fully constrained, whereas a vertical displacement was applied to the top reference point, resulting in the tensile loading of the specimen. The Newton-Raphson method was employed as the solver scheme. The developed model can accurately reproduce the stress-strain experimental curves for both TC-1.0 and TC-1.5 sets (see Fig. 15(c)). A good agreement is also found in terms of failure mode, as shown in Fig. 15(b). The location of the necking region in the model corresponds to that observed in the experiments. No fracture failure in the face sheets of the small-scale sandwich panel tested in edgewise compression was detected. Thus, the reproduction of the fracture failure mode of the coupon specimen is out of the scope of this work.

4.1.2. Core material

The compressive and tensile behaviour of the core of the sandwich

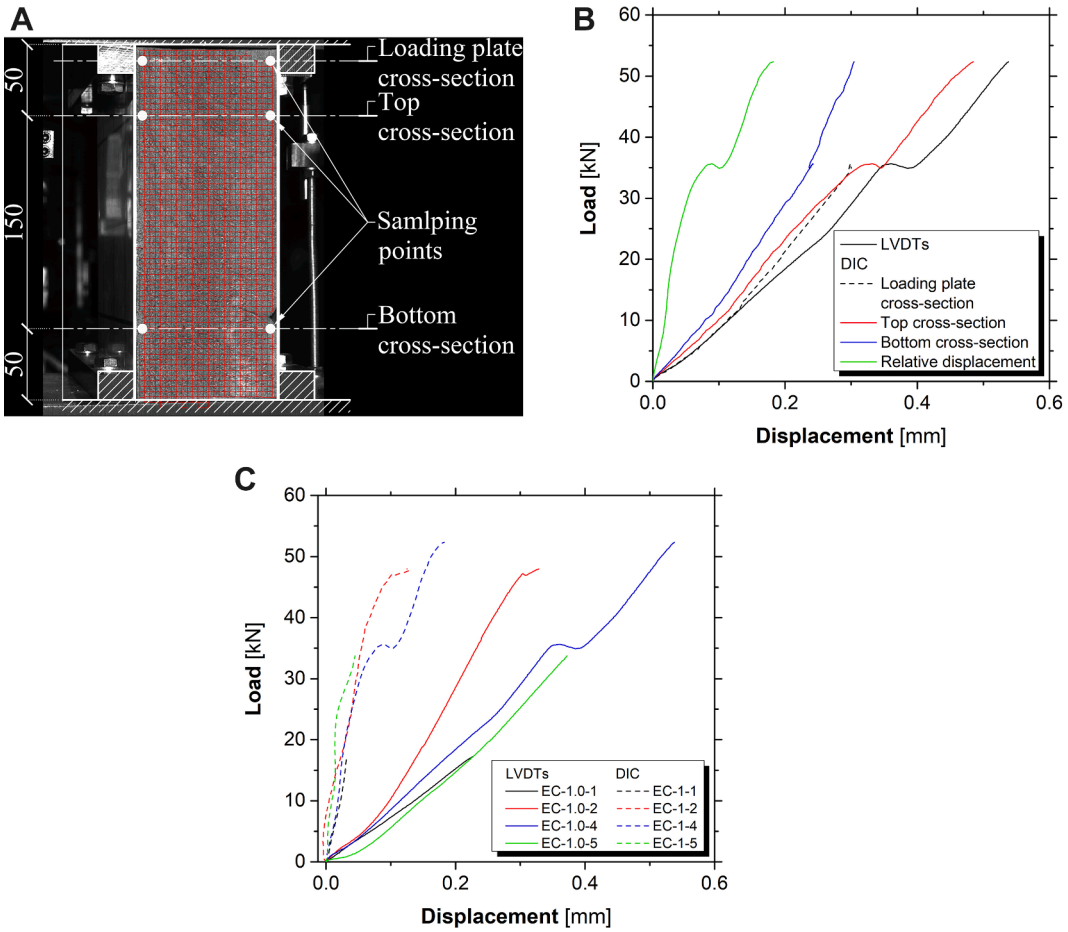

Fig. 14. Edgewise compressive test: (a) location of the monitored points by the DIC; (b) LVDTs and DIC comparison for specimen EC-1.0-4; (c) load-displacement curves based on LVDTs and DIC measurements.

panel is particularly relevant for correctly predicting the instability phenomena, such as wrinkling of the face sheet. The crushable foam material model available in ABAQUS was selected to reproduce the mechanical behaviour of the PUR foam. It requires the definition of the yield surface in the hydrostatic pressure-Von Mises stress space and the true stress-strain curve for uniaxial compressive loading. The parameters needed to define the yield surface were obtained through the method proposed by [48]. It is a simplified calibration process where the yield surface is determined based on the values of the compressive, tensile, and shear yield (τ) strength. No experimental value was available for the shear yield strength. Therefore, the shear yield strength was estimated based on the value of the compressive yield strength. The σ_c/τ ratio ranges from approximately 1.0 to 2.0 according to the values found in the literature on PUR foam core sandwich panels [9,28,49]. Therefore, τ was estimated by dividing σ_c by 1.5. The obtained yield surface is shown in Fig. 16. On the other hand, the formulas to estimate the true stress-true strain curves based on the experimental results were obtained according to [50]. The elastic input parameters are the same for both models, namely $E = 5.71$ MPa and $v = 0.3$. The value of the Poisson's ratio was estimated based on typical average values for polymeric foams found in the literature [51,52]. A numerical model, including material and geometrical nonlinearities, was built to simulate the flatwise compressive and tensile test stress-strain curves (see Fig. 16(b)).

3D continuum solid elements (C3D8R) based on a reduced integration scheme were selected to model the PUR foam core and the steel face sheet. Hexahedral elements with a side length of 6 mm and 3 mm were used to mesh the core and the face sheets, respectively. For what concerns the steel face sheet, a linear elastic material behaviour was assumed. The nodes of the bottom face sheet are tied to a reference point whose degrees of freedom are fully constrained. The compressive and tensile loading is applied by imposing a vertical displacement to the top reference point governing the motion of the nodes of the top face sheet. The same solver scheme as the coupon tensile test model was adopted. The comparison between the average experimental curves and the numerical results is shown in Fig. 17.

The average compressive behaviour of the PUR foam is accurately reproduced up to 0.7 strain (see Fig. 17(a)), which is deemed sufficient for the simulation of the small-scale sandwich panel in edgewise compression. On the other hand, the numerically predicted tensile behaviour shows a nonlinear part of the curve, which was not observed during the experiments. This is an expected result since the Crushable Foam Model does not envisage any failure criteria.

4.2. *Edgewise compressive test*

A FE analysis was conducted to replicate the results of the edgewise compressive tests. The face sheets and the core of the sandwich panels were modelled as described in Sections 4.1.1 and 4.1.2, respectively (see Fig. 18). As debonding could only be observed after failure initiation, the face sheets and the core are assumed to be perfectly bonded. Therefore, a surface-based tie constraint was applied to make the translational motion of the core's outer surface equal to the face sheet's inner surface.

It is worth noting that if the debonding mechanism occurs prior to failure initiation different modelling strategies may be more representative of the real behaviour of the interface. Indeed, cohesive zone modelling (CZM) available in ABAQUS is capable of reproducing the propagation of failure through adhesive interfaces. However, CZM requires the study of the mechanical characteristics of the face sheet-to-

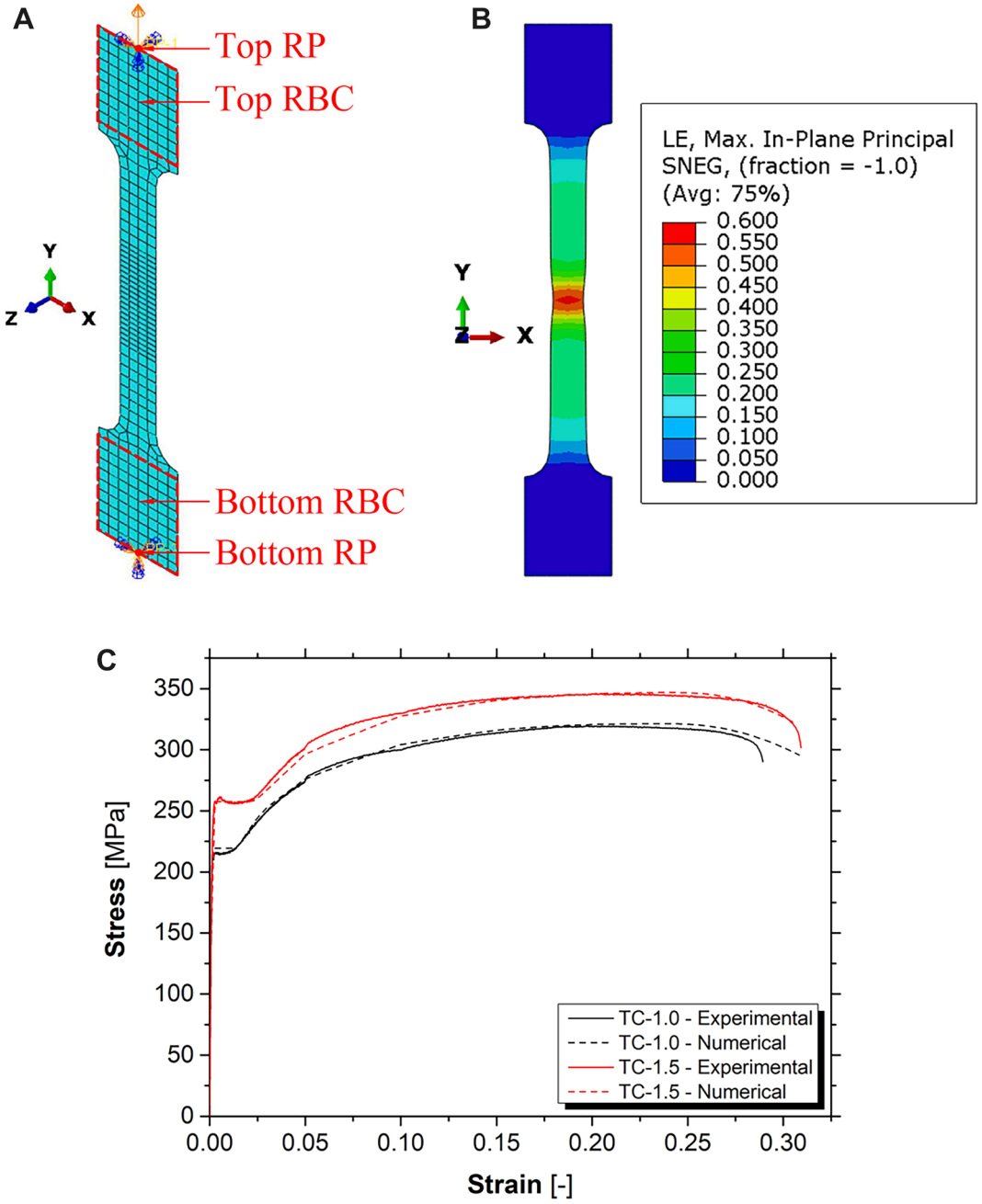

Fig. 15. Tensile coupon test numerical model: (a) mesh; (b) failure mode; (c) comparison of the experimental and numerical stress-strain curves. Notes: RBC – rigid body constraint; RP – reference point.

core interface in terms of stress-traction relationship [44]. The top and bottom nodes of the assembly are tied by means of rigid body constraint to two reference points to which the boundary conditions are applied. All the degrees of freedom of the bottom reference node were constrained, whereas all the degrees of freedom of the top reference node but the vertical translation were constrained. Furthermore, the horizontal translation of the nodes of the area of the face sheets in contact with the solid steel lateral bars is inhibited. Due to the symmetry of the panel and the failure mode (symmetrical wrinkling), only half of the EC-1.0 specimens were simulated, and appropriate boundary conditions were applied to the plane of symmetry. Preliminary buckling analyses were conducted on numerical models of varying mesh sizes. The critical load of the first buckling mode and computational time were used to determine the optimal mesh size. For the nonlinear analyses in Section 4.2.1, a global mesh size of 5 mm was selected (see Fig. 18). Initial geometrical imperfections were introduced in the model to trigger the buckling and failure in the mode shape observed during the experiment, namely wrinkling and global buckling.

4.2.1. *Geometrical imperfections*

Simulation of the imperfection is achieved by means of linear buckling analysis. A unitary load was applied to the top reference point along the vertical direction to retrieve the first tenth-order eigenvalues. The obtained buckling mode shapes were then identified and used to perturb the initial geometry in the subsequent analysis considering nonlinear material and geometrical effect. The linear buckling analysis of specimens EC-1.0 captured buckling mode shapes with fundamentally similar half wavelengths attributed to local buckling. Thus, the first buckling mode (see Fig. 19(a)) with the lowest critical load was applied to the model. Furthermore, the half wavelength of the 1st buckling mode

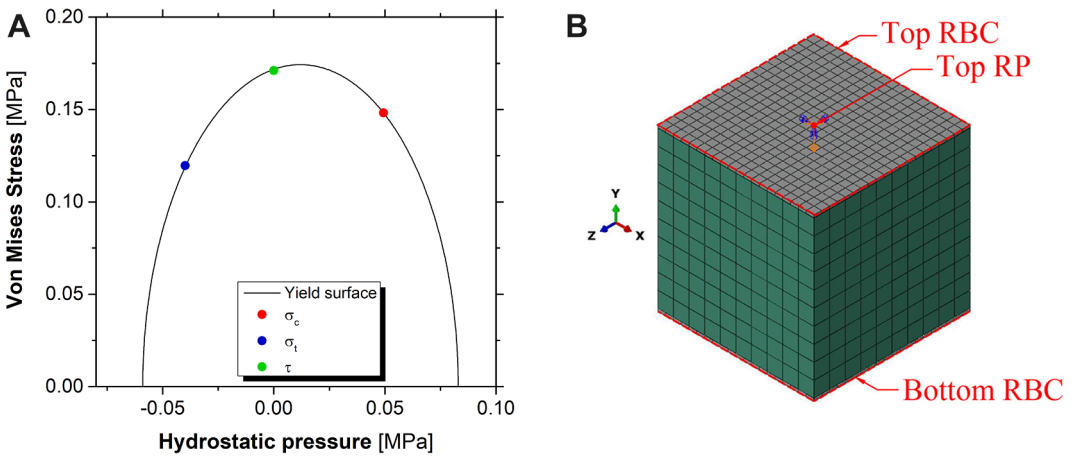

Fig. 16. Flatwise compressive and tensile numerical models: (a) yield surface of the crushable foam material model; (b) mesh. Notes: RBC – rigid body constraint; RP – reference point.

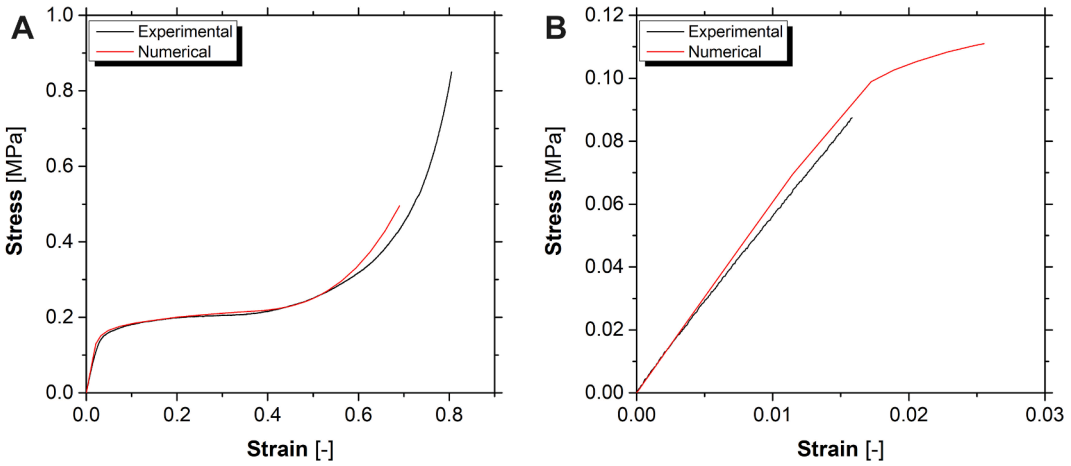

Fig. 17. Comparison of the experimental and numerical stress-strain curves: (a) flatwise compressive test; (b) flatwise tensile test.

(63.8 mm) is in good agreement with the experimental results (-2.7% relative difference). The first two buckling mode shapes of specimens EC-1.5 present significant differences in terms of critical load and half wavelength (see Fig. 19(b) and Fig. 19(c)). Therefore, the two modes were summed together following the recommendations of [53].

Three imperfections magnitude were considered to evaluate the sensitivity of the model to such parameters. The magnitude values were established based on the approach proposed by [54]. According to [53], cumulative distribution function (CFD) values were estimated based on collected data on geometric imperfections of cold-formed steel members. The CFD values connect the probability of occurrence (**P**) with a particular imperfection magnitude. A CDF value is represented as $\mathbf{P}(\Delta<d)$ and indicates the likelihood of a randomly chosen imperfection (Δ) being smaller than a particular imperfection value (d) [53]. For instance, $\mathbf{P}(\Delta<d_1)=75\%$ corresponds to $d_1/t=0.54$ mm, namely a cold-formed steel structural member with a cross-section thickness (t) of 1.0 mm is expected to have an initial local imperfection (d_1) less than 0.54 mm 75% of the time. The magnitudes of the imperfections are related to the thickness of the cross-section and the length of the structural member (L) for what concerns the wrinkling and global buckling, respectively, as reported in Table 4.

Models were developed to simulate the sandwich panels' axial response up to failure initiation, including nonlinear material properties and initial geometrical imperfections. To reproduce the results of the edgewise compressive tests, a vertical displacement of 0.3 mm was prescribed to the top reference node. To assess the influence of the geometrical imperfections on the axial stiffness and peak load of sandwich panels and to retrieve the most appropriate magnitudes and combinations, the numerical results were compared to the experimental curves, as shown in Fig. 20. The vertical displacements were extracted from nodes located in the same positions as those illustrated in Fig. 14 (a).

For what concerns specimens EC-1.0, $\mathbf{P}(\Delta<d_1)=50\%$ yields the most accurate results both in terms of axial stiffness (460.1 kN/mm) and ultimate load (45.5 kN), with a relative difference of -1.7% and +3.2%, respectively. In all cases, the wrinkling failure mode was accurately predicted by the FE models (see Fig. 21(a)).

After a preliminary study on the influence of the 1st buckling mode shape on the model of specimens EC-1.5, $\mathbf{P}(\Delta<d_1)=75\%$ was selected as the adequate magnitude to reproduce the behaviour of the sandwich panels. In the second stage, keeping the magnitude of the 1st buckling mode shape constant, the 2nd buckling mode shape was added to the initial configuration. The amplitudes $\mathbf{P}(\Delta<d_1)=75\%$ and $\mathbf{P}(\Delta<d_2)=75\%$ provide an axial stiffness of 589.9 kN/mm and a peak load of 57.6 kN with a relative difference of +8.3% and less than +0.1%, respectively. Generally, the FE and experimental results show a relative difference of less than 10% and 5% in terms of axial stiffness and peak load, respectively. Nevertheless, small drops and changes in slope are not observed in the numerical curves (see Fig. 20). This could be due to various reasons related to the modelling strategies adopted. The ununiformed ends of the specimens and the corresponding gaps with the loading plate were not reproduced in the numerical environment. The

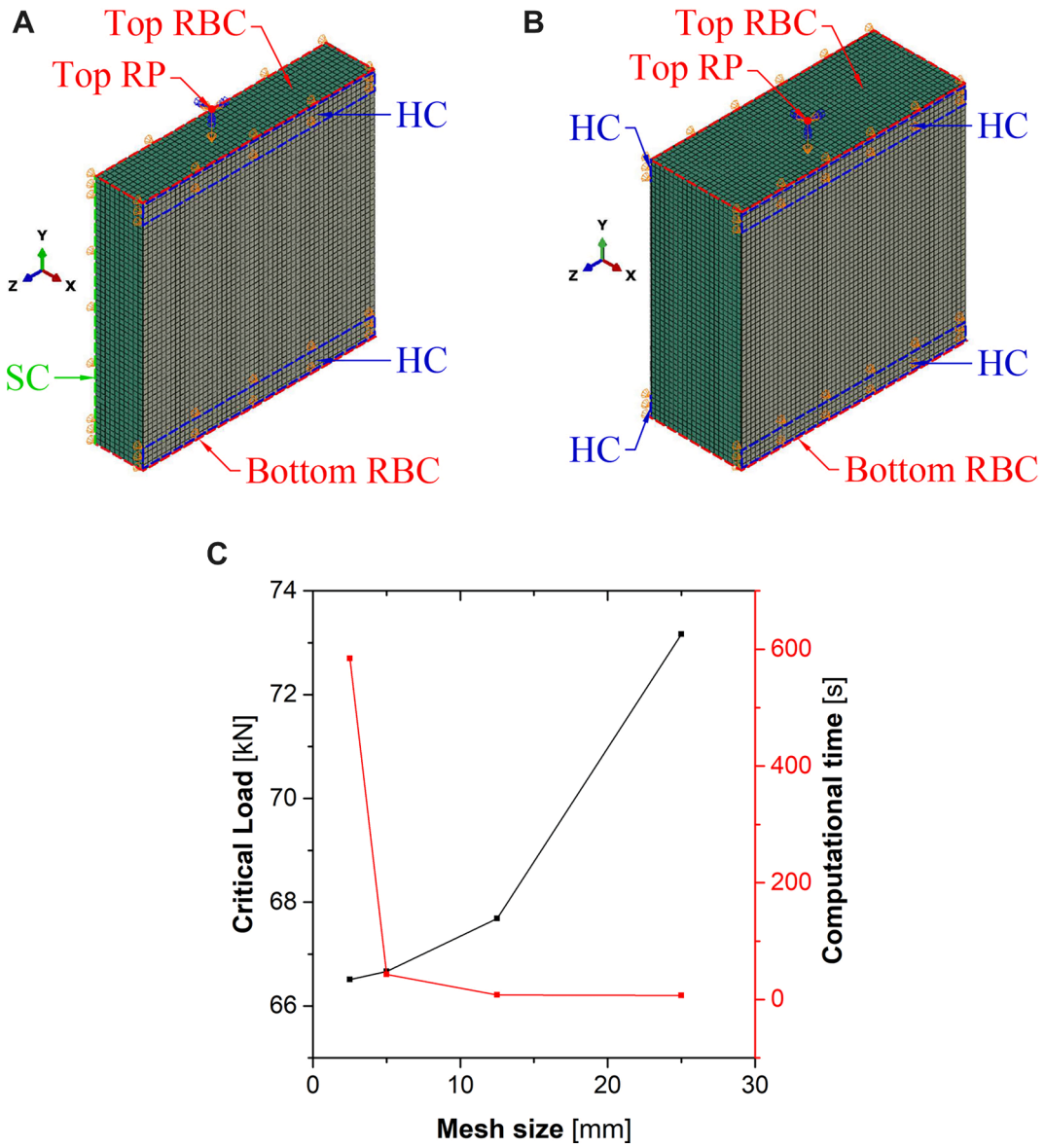

Fig. 18. Edgewise compressive test numerical model: (a) EC-1.0 set; (b) EC-1.5 set; (c) plot of the first critical buckling load for different mesh dimensions. Notes: HC – horizontal constraint; RBC – rigid body constraint; RP – reference point; SC – symmetry constraint.

compressive load is applied through vertical displacement of the top reference node. Additionally, the perfect bond between the face sheets and the core imposed in the numerical model may not be representative of the real interface behaviour. Cracks in the bulk of the PUR foam and/or at the interface with the face sheets may be developing before the peak load is reached. Lastly, the gradient of property through the thickness of the PUR foam observed in the flatwise tensile and compressive tests was not considered in the PUR foam constitutive model, which assumes isotropic behaviour of the material for simplicity. However, there is a good agreement between the numerical and experimental results in terms of deformed shape at failure, as seen in Fig. 21.

5. Analytical modelling

The analytical study carried out in this section considers a sandwich panel of length L and width b with clamped ends subjected to a compressive load P. The sandwich panel comprises face sheets of thickness t_f and a core of thickness t_c. The material properties of the face sheets and core are given in Table 1 and Table 2. The observed experimental response of the sandwich panel loaded in-plane up to failure initiation was generally linear. This linear response is characterised by the sandwich panel stiffness (K_{tot}).

Assuming that the face sheet-to-core interface is perfectly bonded, the axial deflection of the sandwich panel is the same in the face sheet and the core, as given in Equation (1):

$$\delta_{tot} = \delta_f \Leftrightarrow \frac{P \times L}{E_e \times A_{tot}} = \frac{P \times L}{E_f \times A_f} \tag{1}$$

where δ_{tot} is the sandwich panel deformation, δ_f is the axial deformation of the face sheets, A_{tot} is the total cross-section area of the sandwich panel, E_e is the effective Young's modulus of the sandwich panel [55], E_f is the Young's modulus of the face sheets, and A_f is the cross-section area of the face sheets. Keeping in mind that the axial stiffness of a beam subjected to a compressive load is the product of the Young's modulus of the material by the area of the beam divided by its length, and substituting E_e in such equation, yields the sandwich panel stiffness:

$$K_{tot} = \frac{E_e \times A_{tot}}{L} \tag{2}$$

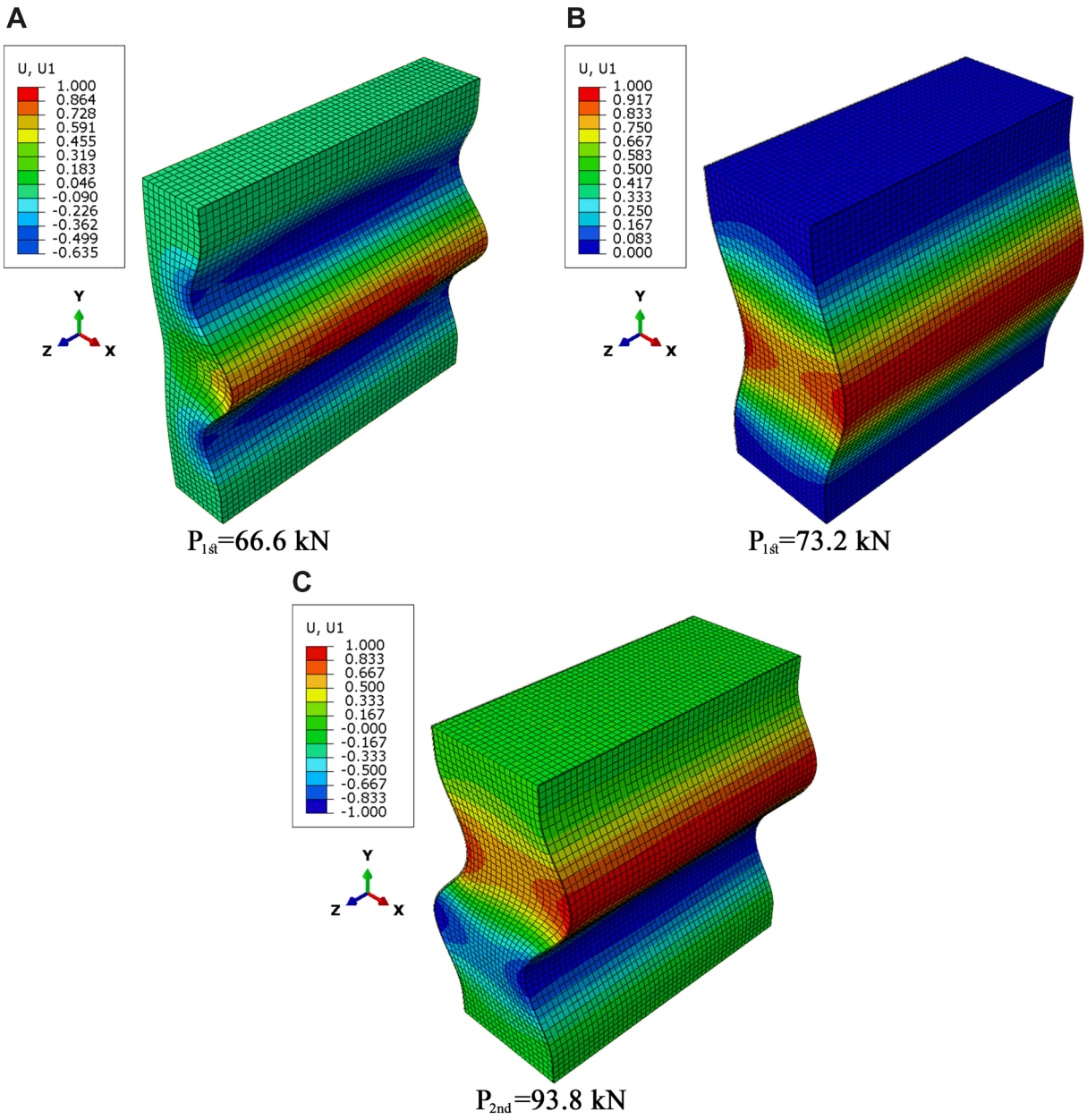

Fig. 19. Buckling eigenvalues and mode shapes: (a) 1st mode of specimen EC-1.0; (b) 1st mode of specimen EC-1.5; (c) 2nd mode of specimen EC-1.5.

Table 4
Statistical magnitude of imperfections.

P(Δ<d)	Wrinkling	Global buckling
	d_1/t	L/d_2
25%	0.17	4755
50%	0.31	2909
75%	0.54	1659

Notes: d_1 – local imperfection; t – plate thickness; d_2 – global imperfection; L – structural member length.

Regarding the prediction of the ultimate load of the sandwich panel, two failure modes are identified: i) global buckling and ii) wrinkling. It is assumed that both EC-1.0 and EC-1.5 sets consist of sandwich panels with thin faces (99% of the bending stiffness is provided by the bending of the face sheets about the centroidal axis of the sandwich panel) and weak cores (bending stiffness of the core about the centroidal axis of the sandwich panel contributes to less than 1% of the total stiffness) [56]. In this case, the global buckling load (P_{cr}) is a combination of the Euler buckling (P_E) and the buckling of the core due to shear (P_s) according to Equation (3):

$$\frac{1}{P_{cr}} = \frac{1}{P_E} + \frac{1}{P_s} \tag{3}$$

The Euler buckling and the core shear buckling are defined by the following expressions:

$$P_E = \frac{\pi^2 \times (E \times I)_{eq}}{(k \times L_e)^2} \tag{4}$$

$$P_s = b \times t_c \times G_c \tag{5}$$

where G_c is the core shear modulus, and L_e is the free length of the sandwich panel between the clamps. Wrinkling occurs when periodic waves in the same magnitude order of the core thickness appear simultaneously all over the surface of the face sheet. Wrinkling may be

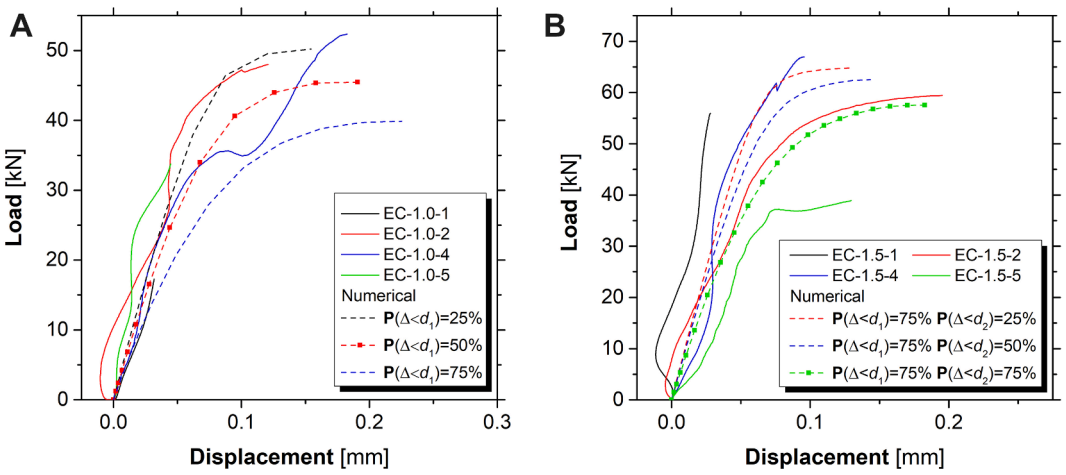

Fig. 20. Comparison between experimental and numerical load-displacement curves: (a) EC-1.0; (b) EC-1.5. Note: The numerical curves with the smallest relative difference from the experiments are highlighted with square symbols.

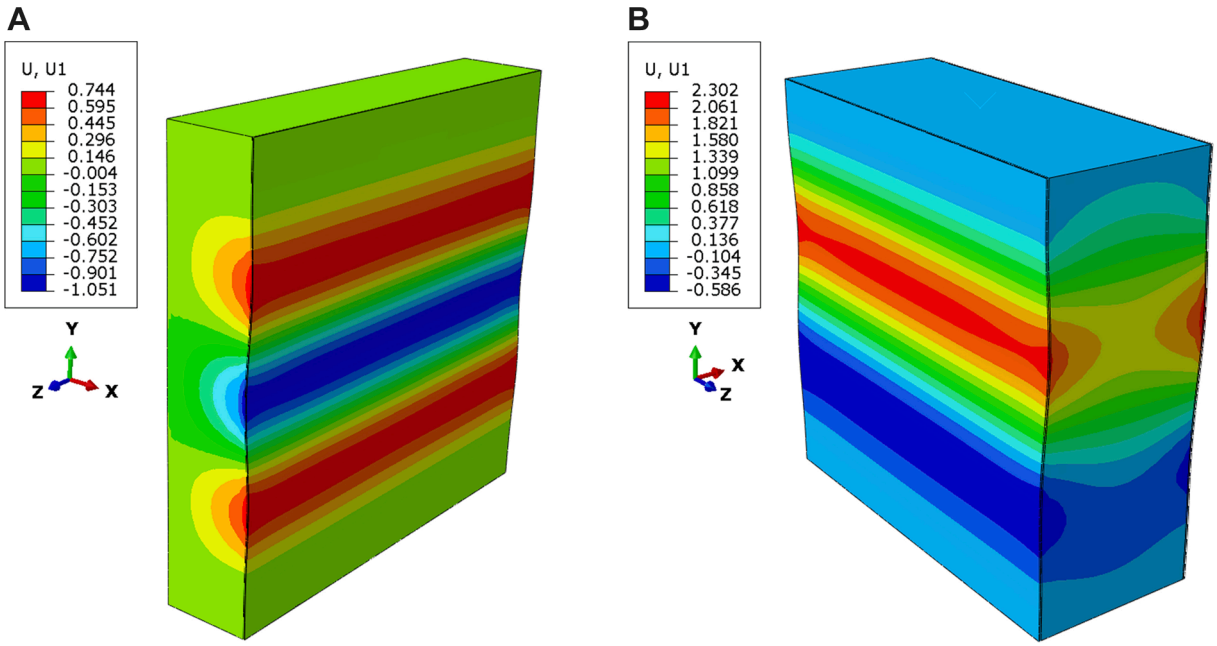

Fig. 21. Out-of-plane displacement at peak load: (a) specimen EC-1.0; (b) specimen EC-1.5.

divided into three categories: i) rigid base (single-sided); ii) antisymmetric; iii) symmetric. In this work, symmetric wrinkling is considered the most appropriate since periodic waves could be observed on both face sheets, as mentioned in Section 3.1.

According to [57] the wrinkling half wavelength (l) and the wrinkling critical stress (σ_w) in the face sheet are given by:

$$l = 1.65 \times t_f \times \sqrt[6]{\frac{E_f^2}{E_c \times G_c}} \tag{6}$$

$$\sigma_w = 0.91 \times \sqrt[3]{E_f \times E\times_c \times G_c} \tag{7}$$

The critical wrinkling load (P_w) will be reached when the face sheets reach the critical wrinkling stress according to Equation (8):

$$P_w = 2 \times b \times t_f \times \sigma_w \tag{8}$$

A summary of the analytical results, along with the experimental values, is presented in Table 5.

Based on Equation (2), the axial stiffnesses are 413.3 kN/mm and

Table 5
Summary of the geometrical properties and predicted and measured failure loads.

Set [-]	L [mm]	c [mm]	t_f [mm]	K_{tot} [kN/mm]	K_{exp} [kN/mm]	P_{cr} [kN]	l [mm]	P_{wr} [kN]	P_{exp} [kN]
EC-1.0	250	100	1.0	413.3	499.0	55.6	64.1	62.9	44.0*
EC-1.5	250	100	1.5	518.0	541.0	55.6	94.2	92.5	57.5

Notes: K_{exp} – average experimental value of the axial stiffness of sandwich panels; P_{exp} – average experimental value of the peak load of sandwich panels; highlighted with "*" is the average wrinkling load of specimens EC-1.0-3, EC-1.0-4, and EC-1.0-5.

581.0 kN/mm for specimens EC-1.0 and EC-1.5, respectively. The analytical predictions are close to the experimental results (the average difference is within 10%). Thus, the assumption of the perfectly bonded interface in the linear stage of the axial response is reasonable. For what concerns the global buckling estimation, G_c is estimated according to the theory of elasticity of isotropic materials [58]. Using Equation (3) resulted in the value of 55.6 kN for both sets of specimens. This is due to the fact that in Equation (3), the buckling of the core due to shear governs the overall failure mode. Indeed, both sets of specimens present the same core characteristics. The global buckling load prediction agrees very well with the average experimental ultimate load of EC-1.5 specimens (-3.4% relative difference). The critical wrinkling load is estimated according to Equation (8), and the values of 62.9 kN and 92.5 kN are obtained for the EC-1.0 and EC-1.5 sets, respectively. Regarding the EC-1.5 set, the critical wrinkling load is higher than the global buckling load, confirming the consistency observed in the failure mode of EC-1.5 specimens. On the other hand, the predicted critical wrinkling load differs from the average experimental ultimate load of the EC-1.0 specimens that failed due to wrinkling (44.0 kN). Nevertheless, different values of the constant coefficient of Equation (7) were proposed by several authors ranging from 0.5 to 0.91 [57,59]. These coefficients were changed to fit the experimental results and may not be appropriate for the sandwich panel studied in this work. Indeed, a coefficient of 0.65 would result in a wrinkling load of 44.9 kN and 66.1 kN for the EC-1.0 and EC-1.5 specimens, respectively. Such results would implicate the occurrence of global buckling in the EC-1.5 specimens and, simultaneously, reduce the difference with the experimental average peak load of the EC-1.0 specimens. The wrinkling half wavelength calculated according to Equation (6) yields a value of 64.1 mm for the EC-1.0 specimens. The analytical prediction agrees well with the experimental results (-2.2% relative difference) despite the discrepancy in terms of ultimate load. Such difference may also be explained by the presence of geometrical imperfections, which affect the ultimate load rather than the shape of the instability mode.

6. Discussion of the results

The experimental setup of the edgewise compressive test followed the recommendations of the standard ASTM C364 (1999) [43]. The lateral solid steel bar proved effective in restricting the outward buckling of the face sheets in the vicinity of the loading and support plates. Nevertheless, some specimens presented inward buckling of the face sheets and, consequently, foam crushing prior to failure initiation. The insertion of a solid steel block in the core at the ends of the sandwich panel [20] may be beneficial to avoid such premature failures. The specimens EC-1.0 and EC-1.5 subjected to edgewise compressive loading displayed an axial stiffness approximately 7 and 8 times higher than those with similar dimensions but different face sheet materials tested in [9]. It is a promising result in view of their application as primary structural floor elements. Adequate axial stiffness is particularly relevant in seismic-prone areas where the floor shall act as a diaphragm, equally redistributing the horizontal actions to the vertical structures. For what concerns the failure propagation of the sandwich panels, most of the tested specimens ultimately failed due to debonding between the top face sheet and the core. This may suggest that the current manufacturing process generates a different foam micro-structure through the thickness of the panel. Nevertheless, the assumption of the PUR foam as an isotropic material yields discretely accurate numerical results up to failure initiation. The possibility of modelling layers of PUR foam with different mechanical properties may be considered in future studies to reproduce the post-peak behaviour of the sandwich panels. Furthermore, the failure mode of the EC-1.5 specimens is governed by the buckling of the core due to shear. However, the shear properties of the core were estimated according to the theory of elasticity and on typical values found in the literature. An experimental campaign to validate the prediction of the shear properties shall be considered to predict the composite structure's behaviour more accurately.

The developed numerical models can accurately predict the behaviour of the sandwich panels up to failure initiation. Nevertheless, a calibration procedure against the experimental results is required to select appropriate buckling mode shapes and their magnitudes to be used as initial geometrical imperfections. The comparison of the imperfection magnitudes with other authors' works is not straightforward. Numerical studies have been focused on composite face sheets sandwich panels and the simulation of debonding failure mode without including the magnitude of the initial imperfections [17,60,61]. A good agreement was found between the experimental, numerical, and analytical results, as shown in Table 6.

The most significant difference is found between the analytically predicted wrinkling load and the experimental average peak load. Nevertheless, it is common in the literature to adapt the constant coefficient of Equation (7) to better fit the experimental results. For the sandwich panel objects of this study, a coefficient of 0.65 produces more accurate results. Higher wrinkling load predictions than the measured ones are also reported in [20]. It is suggested that the analytical models consider a perfect geometry and do not reflect the high sensitivity of the actual structure to geometrical imperfections.

7. Conclusions

In this paper, a comprehensive study on the structural behaviour of in-plane loaded sandwich panels is presented, including experimental, numerical, and analytical approaches. Through an accurate literature review, adequate experimental procedures were selected and developed for the mechanical characterisation of the constituent materials and the small-scale sandwich panels. Recommendations are proposed to complement the procedures described in the standards based on the obtained experimental results: i) the use of spherical washers and 3D bearing joints to avoid bending moments in the flatwise compressive and tensile tests; ii) the use of stiffening blocks in the ends of small-scale sandwich panels in the edgewise compressive test. EC-1.0 and EC-1.5 sets show promising results in terms of axial stiffness and peak load. The accuracy of the developed constitutive models also confirms the experimental procedures' quality. The numerical simulations of the material characterisation tests are quite precise in reproducing the experimental curves. The lack of experimental data on the shear properties of the core is addressed, and the estimated values result from a thorough literature review. Nevertheless, future studies shall be carried out to validate those assumptions. The numerical models developed for specimens EC-1.0 and EC-1.5 can reproduce the behaviour of the sandwich panels up to failure initiation. The sensitivity of the models to initial geometrical imperfections is assessed through parametric studies. The buckling mode shapes and the corresponding magnitudes which yield the most accurate results are successfully identified. Finally, the analytical models show a good correlation with the experimental results of specimens EC-1.5. On

Table 6
Comparison of experimental, numerical, and analytical results of the edgewise compressive test.

Approach [-]	K [kN/mm]		P_{wr} [kN]	l [mm]	P_{cr} [kN]
	EC-1.0	**EC-1.5**	**EC-1.0**	**EC-1.0**	**EC-1.5**
Experimental	468.0	541.0	44.0*	65.5	57.5
Numerical	460.1 (-1.7%)	589.9 (+8.3%)	45.5 (+3.2%)	63.8 (-2.7%)	57.6 (+0.2%)
Analytical	413.3 (-13.2%)	581.0 (+6.9%)	44.9** (+2.0%)	64.1 (-2.2 %)	55.6 (-3.4%)

Notes: the values between parentheses are the corresponding relative differences; highlighted with "*" is the average wrinkling load of specimens EC-1.0-3, EC-1.0-4, and EC-1.0-5; highlighted with "**" is the predicted wrinkling load with the constant coefficient set equal to 0.65.

the other hand, a significant difference in the estimation of the peak load of EC-1.0 specimens is found. A correction to the formula's coefficient is therefore proposed in line with the work of other authors.

CRediT authorship contribution statement

Pier Giovanni Benzo: Investigation, Formal analysis, Writing – original draft. **João M. Pereira:** Validation, Supervision, Funding acquisition, Methodology, Project administration, Formal analysis, Conceptualization, Investigation, Writing – review & editing. **José Sena-Cruz:** Conceptualization, Methodology, Supervision, Writing – review & editing.

Declaration of Competing Interest

The authors declare that they have no known competing financial interests or personal relationships that could have appeared to influence the work reported in this paper.

Data availability

Data will be made available on request.

Acknowledgements

This work was developed within the scope of the research project "Lightslab – Desenvolvimento de soluções inovadoras de lajes de painel sandwich", supported by FEDER funds through the Operational Program for Operational Program for Competitiveness and Internationalization (POCI) and the Portuguese National Innovation Agency (ANI) – project no. 33865 [POCI-01-0247-FEDER-033865]. This work was partly financed by FCT / MCTES through national funds (PIDDAC) under the R&D Unit Institute for Sustainability and Innovation in Structural Engineering (ISISE), under reference UIDB / 04029/2020, and under the Associate Laboratory Advanced Production and Intelligent Systems ARISE under reference LA/P/0112/2020. This work is financed by national funds through FCT – Foundation for Science and Technology, under grant agreement 2020.08319.BD attributed to the 1st author.

References

[1] L. CoDyre, A. Fam, The effect of foam core density at various slenderness ratios on axial strength of sandwich panels with glass-FRP skins, Compos. B Eng. 106 (Dec. 2016) 129–138, https://doi.org/10.1016/j.compositesb.2016.09.016.
[2] J.M. Davies, Lightweight Sandwich Construction, Blackwell Science, Oxford, 2001.
[3] D. Zenkert, The Handbook of Sandwich Construction, Engineering Materials Advisory Services, Worcestershire, 1997.
[4] A. Fam, T. Sharaf, Flexural performance of sandwich panels comprising polyurethane core and GFRP skins and ribs of various configurations, Compos. Struct. 92 (12) (Nov. 2010) 2927–2935, https://doi.org/10.1016/j.compstruct.2010.05.004.
[5] H. Abdolpour, J. Garzón-Roca, G. Escusa, J.M. Sena-Cruz, J.A.O. Barros, I. B. Valente, Development of a composite prototype with GFRP profiles and sandwich panels used as a floor module of an emergency house, Compos. Struct. 153 (Oct. 2016) 81–95, https://doi.org/10.1016/j.compstruct.2016.05.069.
[6] ESPON 2020, Policy Brief - Reuse of spaces and buildings. European Spatial Planning Observation Network, 2020.
[7] P. Sharafi, S. Nemati, B. Samali, A. Mousavi, S. Khakpour, Y. Aliabadizadeh, Edgewise and flatwise compressive behaviour of foam-filled sandwich panels with 3-D high density polyethylene skins, Eng. Solid Mech. 6 (3) (2018) 285–298, https://doi.org/10.5267/j.esm.2018.3.005.
[8] A. Montazeri, M. Safarabadi, A comparative study on adding chopped kenaf fibers to the core of glass/epoxy laminates under quasi-static indentation: experimental and numerical approaches, J. Compos. Mater. 56 (25) (2022) 3821–3833, https://doi.org/10.1177/00219983221124204.
[9] J.R. Correia, M. Garrido, J.A. Gonilha, F.A. Branco, L.G. Reis, GFRP sandwich panels with PU foam and PP honeycomb cores for civil engineering structural applications: effects of introducing strengthening ribs, Int. J. Struct. Integrity 3 (2) (2012) 127–147, https://doi.org/10.1108/17579861211235165.
[10] P. Sharafi, S. Nemati, B. Samali, M. Ghodrat, Development of an innovative modular foam-filled panelized system for rapidly assembled postdisaster housing, Buildings 8 (8) (Jul. 2018), https://doi.org/10.3390/buildings8080097.
[11] Z.K. Awad, T. Aravinthan, Y. Zhuge, Experimental and numerical analysis of an innovative GFRP sandwich floor panel under point load, Eng. Struct. 41 (Aug. 2012) 126–135, https://doi.org/10.1016/j.engstruct.2012.03.023.
[12] N.J. Mills, Polymer foams handbook: engineering and biomechanics applications and design guide, Butterworth Heinemann, 2007.
[13] C.R. Briscoe, S.C. Mantell, T. Okazaki, J.H. Davidson, Local shear buckling and bearing strength in web core sandwich panels: model and experimental validation, Eng. Struct. 35 (Feb. 2012) 114–119, https://doi.org/10.1016/j.engstruct.2011.10.020.
[14] S.C. Mantell, G.L. Di Muoio, J.H. Davidson, C.K. Shield, B.J. Siljenberg, T. Okazaki, Panelized residential roof system. I: structural design, J. Archit. Eng. 23 (4) (Dec. 2017), https://doi.org/10.1061/(asce)ae.1943-5568.0000277.
[15] B. Kraus, R. Das, B. Banerjee, Anisotropy and variability in polyurethane foams: experiments and modeling, 2013.
[16] M. Chuda-Kowalska, A. Garstecki, Experimental and numerical analyses of anisotropic behaviour of PU foam, in ECCM16 Conference, Plastics, Rubber and Composites, Sevilla, Jun. 2016.
[17] N. Mitra, B.R. Raja, Improving delamination resistance capacity of sandwich composite columns with initial face/core debond, Compos. B Eng. 43 (3) (Apr. 2012) 1604–1612, https://doi.org/10.1016/j.compositesb.2011.11.039.
[18] M. Mohamed, S. Anandan, Z. Huo, V. Birman, J. Volz, K. Chandrashekhara, Manufacturing and characterization of polyurethane based sandwich composite structures, Compos. Struct. 123 (May 2015) 169–179, https://doi.org/10.1016/j.compstruct.2014.12.042.
[19] N.A. Fleck, I. Sridhar, End compression of sandwich columns, Compos. A Appl. Sci. Manuf. 33 (3) (2002) 353–359, https://doi.org/10.1016/S1359-835X(01)00118-X.
[20] F. Cote, R. Biagi, H. Bart-Smith, V.S. Deshpande, Structural response of pyramidal core sandwich columns, Int. J. Solids Struct. 44 (10) (May 2007) 3533–3556, https://doi.org/10.1016/j.ijsolstr.2006.10.004.
[21] A.G. Mamalis, D.E. Manolakos, M.B. Ioannidis, D.P. Papapostolou, On the crushing response of composite sandwich panels subjected to edgewise compression: experimental, Compos. Struct. 71 (2) (Nov. 2005) 246–257, https://doi.org/10.1016/j.compstruct.2004.10.006.
[22] M. Safarabadi, M. Haghighi-Yazdi, M.A. Sorkhi, A. Yousefi, Experimental and numerical study of buckling behavior of foam-filled honeycomb core sandwich panels considering viscoelastic effects, J. Sandw. Struct. Mater. 23 (8) (2021) 3985–4015, https://doi.org/10.1177/1099636220975168.
[23] A.C. Berg, L.C. Bank, M.G. Oliva, J.S. Russell, Construction and cost analysis of an FRP reinforced concrete bridge deck, Constr. Build. Mater. 20 (8) (Oct. 2006) 515–526, https://doi.org/10.1016/j.conbuildmat.2005.02.007.
[24] X. Wang, Z. Wu, Evaluation of FRP and hybrid FRP cables for super long-span cable-stayed bridges, Compos. Struct. 92 (10) (Sep. 2010) 2582–2590, https://doi.org/10.1016/j.compstruct.2010.01.023.
[25] C. Burgoyne, I. Balafas, Why is frp not a financial success?, in 8th International Symposium on Fiber Reinforced Polymer Reinforcement for Reinforced Concrete Structures, Patras, Jul. 2007.
[26] P.G. Benzo, J.M. Pereira, J. Sena-Cruz, Optimization of steel web core sandwich panel with genetic algorithm, Eng. Struct. 253 (Feb. 2022), https://doi.org/10.1016/j.engstruct.2021.113805.
[27] Decreto-Lei n.º 118/2013, Sistema de Certificação Energética dos Edifícios – Regulamento de Desempenho Energético dos Edifícios de Habitação – Regulamento de Desempenho Energético dos Edifícios de Comércio e Serviços. Ministério da Economia e do Emprego, 2013.
[28] A. Shams, A. Stark, F. Hoogen, J. Hegger, H. Schneider, Innovative sandwich structures made of high performance concrete and foamed polyurethane, Compos. Struct. 121 (Mar. 2015) 271–279, https://doi.org/10.1016/j.compstruct.2014.11.026.
[29] EN ISO 6892-1:2016, Metallic materials - Tensile testing - Part 1: Method of test at room temperature. European Committee for Standardization, 2016.
[30] P.G. Benzo, J. Sena-Cruz, J.M. Pereira, P.B. Lourenço, 'Definição de requisitos e especificaçoes tecnicas do produto', Dec. 2018.
[31] Y. Huang, B. Young, The art of coupon tests, J. Constr. Steel Res. 96 (May 2014) 159–175, https://doi.org/10.1016/j.jcsr.2014.01.010.
[32] EN 10346:2015, Continuously hot-dip coated steel flat products for cold forming - Technical delivery conditions. European Committee for Standardization, 2015.
[33] F.J. Meza, J. Becque, I. Hajirasouliha, Experimental study of the cross-sectional capacity of cold-formed steel built-up columns, Thin-Walled Struct. 155 (Oct. 2020), https://doi.org/10.1016/j.tws.2020.106958.
[34] Astm e178–21,, Standard Practice for Dealing With Outlying Observations, ASTM International, 2021.
[35] Astm c365, c365m-22,, Standard Test Method for Flatwise Compressive Properties of Sandwich Cores, ASTM International, 2022.
[36] ASTM C297-94(1999), Standard Test Method for Flatwise Tensile Strength of Sandwich Constructions. 2017.
[37] A.D. Marter, A.S. Dickinson, F. Pierron, M. Browne, A practical procedure for measuring the stiffness of foam like materials, Exp. Tech. 42 (2018) 439–452, https://doi.org/10.1007/s40799-018-0247-0.
[38] H. Tuwair, J. Drury, J. Volz, Testing and evaluation of full scale fiber-reinforced polymer bridge deck panels incorporating a polyurethane foam core, Eng. Struct. 184 (Apr. 2019) 205–216, https://doi.org/10.1016/j.engstruct.2019.01.104.
[39] V.S. Deshpande, N.A. Fleck, Multi-axial yield behaviour of polymer foams, Acta Mater. 49 (10) (2001) 1859–1866.
[40] M.C. Hawkins, B. O'Toole, D. Jackovich, Cell morphology and mechanical properties of rigid polyurethane foam, J. Cell. Plast. 41 (3) (May 2005) 267–285, https://doi.org/10.1177/0021955X05053525.

[41] G. Odian, Principles of Polymerization, 4th ed., John Wiley & Sons Inc, Hoboken, 2004.
[42] M.F. Ashby, R.F.M. Medalist, The mechanical properties of cellular solids, Metall. Trans. A 14 (1983) 1755–1769, https://doi.org/10.1007/BF02645546.
[43] Astm c364, c364m-16,, Standard Test Method for Edgewise Compressive Strength of Sandwich Constructions, ASTM International, 2016.
[44] B. Kraus, R. Das, B. Banerjee, Characterization of cohesive laws for foam-metal interfaces, Int. J. Appl. Mech. 6 (6) (2014) pp, https://doi.org/10.1142/S1758825114500720.
[45] H. Schreier, J.J. Orteu, M.A. Sutton, Image correlation for shape, motion and deformation measurements: Basic concepts, theory and applications. Springer US, 2009. 10.1007/978-0-387-78747-3.
[46] P. Arasaratnam, K.S. Sivakumaran, M.J. Tait, True stress-true strain models for structural steel elements, ISRN Civil Eng. 2011 (Aug. 2011) 1–11, https://doi.org/10.5402/2011/656401.
[47] H.C. Ho, K.F. Chung, X. Liu, M. Xiao, D.A. Nethercot, Modelling tensile tests on high strength S690 steel materials undergoing large deformations, Eng. Struct. 192 (Aug. 2019) 305–322, https://doi.org/10.1016/j.engstruct.2019.04.057.
[48] I. Carranza, et al., Characterising and modelling the mechanical behaviour of polymeric foams under complex loading, J. Mater. Sci. 54 (16) (Aug. 2019) 11328–11344, https://doi.org/10.1007/s10853-019-03673-8.
[49] T. Sharaf, A. Fam, Analysis of large scale cladding sandwich panels composed of GFRP skins and ribs and polyurethane foam core, Thin-Walled Struct. 71 (2013) 91–101, https://doi.org/10.1016/j.tws.2013.05.006.
[50] D.A. Şerban, R. Negru, H. Filipescu, L. Marşavina, Investigations on the influence of the triaxial state of stress on the failure of polyurethane rigid foams, Contin. Mech. Thermodyn. (2020), https://doi.org/10.1007/s00161-020-00924-x.
[51] J.B. Choi, R.S. Lakes, Non-linear properties of polymer cellular materials with a negative Poisson's ratio, J. Mater. Sci. 27 (1992) 4678–4684, https://doi.org/10.1007/BF01166005.
[52] R.D. Widdle, A.K. Bajaj, P. Davies, Measurement of the Poisson's ratio of flexible polyurethane foam and its influence on a uniaxial compression model, Int. J. Eng. Sci. 46 (1) (Jan. 2008) 31–49, https://doi.org/10.1016/j.ijengsci.2007.09.002.
[53] B.W. Schafer, T. Peköz, Computational modeling of cold-formed steel: characterizing geometric imperfections and residual stresses, J. Constr. Steel Res. 47 (3) (1998) 193–210, https://doi.org/10.1016/S0143-974X(98)00007-8.
[54] V.M. Zeinoddini, B.W. Schafer, Simulation of geometric imperfections in cold-formed steel members using spectral representation approach, Thin-Walled Struct. 60 (Nov. 2012) 105–117, https://doi.org/10.1016/j.tws.2012.07.001.
[55] A. Lindström, L. Lindström, S. Hallström, H. Hallström, Energy absorption of sandwich panels subjected to in-plane loads, in ASME 8th Biennial Conference on Engineering Systems Design and Analysis, Torino, Jul. 2006, pp. 739–747. 10.1115/ESDA2006-95771.
[56] H.G. Allen, Analysis and design of structural sandwich panels, Pergamon Press, Oxford, 1969.
[57] N.J. Hoff, S.E. Mautner, The buckling of sandwich-type panels, J. Aeronautical Sci. 12 (3) (Jul. 1945) 285–297, https://doi.org/10.2514/8.11246.
[58] S. Timoshenko, J.N. Goodier, Theory of Elasticity, McGraw Hill, New York, 1951.
[59] M.A. Mousa, N. Uddin, Structural behavior and modeling of full-scale composite structural insulated wall panels, Eng. Struct. 41 (Aug. 2012) 320–334, https://doi.org/10.1016/j.engstruct.2012.03.028.
[60] A. Lindström, S. Hallström, In-plane compression of sandwich panels with debonds, Compos. Struct. 92 (2) (Jan. 2010) 532–540, https://doi.org/10.1016/j.compstruct.2009.08.039.
[61] A.G. Mamalis, K.N. Spentzas, D.P. Papapostolou, N. Pantelelis, Finite element investigation of the influence of material properties on the crushing characteristics of in-plane loaded composite sandwich panels, Thin-Walled Struct. 63 (2013) 163–174, https://doi.org/10.1016/j.tws.2012.09.011.